CHAPTER 23

Microtubule and MAPs: Thermodynamics of Complex Formation by AUC, ITC, Fluorescence, and NMR

François Devred[*], Pascale Barbier[*], Daniel Lafitte[*], Isabelle Landrieu[†], Guy Lippens[†], *and* Vincent Peyrot[*]

[*]CRO2, U911 Inserm, Aix-Marseille Université, 27 Bd Jean Moulin, 13385 Marseille cedex 05, France

[†]CNRS-UMR 8576 UGSF-IFR 147, Université des Sciences et Technologies de Lille 1, 59655 Villeneuve d'Ascq Cedex, France

Abstract

Microtubules are implicated in many essential cellular processes such as architecture, cell division, and intracellular traffic, due to their dynamic instability. This dynamicity is tightly regulated by microtubule-associated proteins (MAPs), such as

METHODS IN CELL BIOLOGY, VOL. 95

978-0-12-374815-7
DOI: 10.1016/S0091-679X(10)95023-1

tau and stathmin. Despite extensive studies motivated by their central role in physiological functions and pathological role in neurodegenerative diseases and cancer, the precise mechanisms of tau and stathmin binding to tubulin and their consequences on microtubule stability are still not fully understood. One of the most crucial points missing is a quantitative thermodynamic description of their interaction with tubulin/microtubules and of the tubulin complexes formed upon these interactions. In this chapter, we will focus on the use of analytical ultracentrifugation, isothermal titration calorimetry, and nuclear magnetic resonance—three powerful and complementary techniques in the field of MAP–tubulin/microtubule interactions, in addition to the spectrometric techniques and co-sedimentation approach. We will present the limits of these techniques to study this particular interaction and precautions that need to be taken during MAPs preparation. Understanding the molecular mechanisms that govern MAPs action on microtubular network will not only shed new light on the role of this crucial family of protein in the biology of the cell, but also hopefully open new paths to increase the therapeutic efficiency of microtubule-targeting drugs in cancers therapies and neurodegeneratives diseases prevention.

I. Introduction

The microtubule cytoskeleton is a very dynamic network that plays a crucial role in many cellular processes such as cellular architecture, cell division, and intracellular traffic. Microtubules (MTs) are implicated in all of these processes because of their ability to constantly switch from polymerization to depolymerization, a phenomenon known as dynamic instability, which enables their structural rearrangement, and reactivity to cellular signaling. Microtubules and their functions are tightly regulated by a great number of proteins known as microtubule-associated proteins (MAPs), which can bind to free tubulin and/or to MTs. MAPs can be divided in two groups depending on their activity on MT formation. Stabilizing MAPs, such as tau, preferentially bind to MTs and favor their polymerization, whereas destabilizing MAPs, such as stathmin, bind to both free tubulin and MTs, promoting MT depolymerization. Tau and stathmin are the two most studied MAPs because of their central role in physiological functions and also because of their implications in neurodegenerative diseases and cancer.

Tau is a MAP that stabilizes axonal microtubules and maintains neuronal processes (Cleveland *et al.*, 1977). Human brain expresses six tau isoforms that are generated from a single gene by alternative mRNA splicing. The longest four-repeat 441 amino acids isoform of tau, htau40, was used throughout our biophysical studies. Beyond its physiological role as a MT-stabilizing protein, tau is also known to play a major role in Alzheimer disease (Trojanowski and Lee, 2002). Upon phosphorylation, tau detaches from microtubules and, after subsequent hyperphosphorylation, aggregates into pathological paired helical filaments (PHFs). Even though many kinases-targeting tau have been discovered and multiple phosphorylation sites studied (Biernat *et al.*, 1992; Goedert *et al.*, 1994; Goedert *et al.*, 1995; Hasegawa *et al.*, 1992; Hoffmann *et al.*, 1997; Mercken *et al.*, 1992; Zheng-Fischhofer *et al.*, 1998), the precise mechanisms of tau dissociation from MTs and subsequent aggregation are still not fully understood. Several models have been

proposed to explain how tau proteins interact with MTs, using different stoichiometry, binding affinity, and geometry of tau. In addition to the fact that no unifying scheme has been proposed, the quantification of the influence of other factors, such as the oxidation state of the two cysteines of tau in addition to its posttranslational modification by phosphorylation, remains challenging.

Stathmin, also designated as oncoprotein 18 among other names, is a MAP that destabilizes microtubules and plays a role in many cellular processes including migration and cell division. Stathmin and related protein family members that share the same stathmin-like domain (SLD), such as RB3, promote MT depolymerization by increasing the catastrophe rate of MTs (transition from a state of polymerization to a state of depolymerization) and by sequestering free tubulin, thus lowering the pool of "assembly competent" tubulin (Charbaut *et al.*, 2001). Stathmin activity/binding to tubulin is also tightly regulated by phosphorylation. For example, during cell division, as cells enter mitosis, stathmin is inactivated by phosphorylation allowing microtubules to form the mitotic spindle. As cells exit mitosis, stathmin is activated by dephosphorylation, leading to depolymerization of the mitotic spindle and proper separation of the daughter cells. Over the past 20 years it has been shown that stathmin is expressed at high levels in a wide variety of human cancers, including breast cancer, leukemia, lymphoma, prostate, and ovarian carcinoma (Curmi *et al.*, 2000; Friedrich *et al.*, 1995; Ghosh *et al.*, 2007; Price *et al.*, 2000) suggesting that it could play a role in tumor progression. Furthermore, several studies have shown a correlation between the level of expression of stathmin in cancer cells and their sensitivity to microtubule-targeting agents (Alli *et al.*, 2002; Alli *et al.*, 2007a,b; Iancu *et al.*, 2000; Martello *et al.*, 2003; Mistry *et al.*, 2007; Xi *et al.*, 2009). Despite all these clinical and cellular studies, there is no clear understanding of the exact role of this MAP in tumor progression and in tumor cells sensitivity to anticancer drugs. Significant progress has been made in the understanding of stathmin interaction to tubulin with the resolution of the T2S complex (two molecules of tubulin and one stathmin) structure by X-ray crystallography (Gigant *et al.*, 2000). Even though it confirmed the stoichiometry of the T2S complex and validated the model, this structure did not, however, answer all the questions about stathmin–tubulin interaction thermodynamics.

Binding of both tau and stathmin to MTs plays a pivotal role in both pathological and physiological processes. Understanding the mechanisms of MAPs requires a quantitative description of the interaction of tubulin and/or microtubules with MAPs in different states of phosphorylation, and of the effects of these MAPs in the different states of MT dynamics. This chapter will focus on the methods that we have used to measure the thermodynamic parameters of the interaction of tau or stathmin with tubulin. These methods enabled us to generate new insights into how MAPs interact with tubulin and/or MTs at the molecular level and to address the following questions. What are the consequences of MAP binding on the oligomeric state of tubulin? What is the nature of the interaction between MT and its MAPs? How is this interaction regulated and which regions of the proteins are involved?

Understanding the molecular mechanisms that govern MAPs action on MT network will not only shed new light on the role of this crucial family of proteins in the biology of the cell, but also hopefully open new avenues to increase the therapeutic efficacy of microtubule-targeting drugs in cancer therapies and neurodegenerative disease prevention.

II. Rationale

Various methods are routinely used to measure the thermodynamic parameters of complexes formation between two proteins in solution; each method having its pros and cons depending on the stability of the complex and on the nature of the information that we are seeking. Measure of thermodynamic parameters relies on being able to follow the formation of a complex, which often means distinguishing between free or bound ligand and tubulin.

It is important to remember that an accurate description of the percentage of complexes formed thereby is only possible when the absolute concentrations of both partners are of the same order of magnitude than the dissociation constant (K_d). Nevertheless, even in those borderline cases, the methods can indicate changes in affinity caused by different parameters. In the following paragraphs, we will detail several biophysical methods to detect and characterize the MAP/tubulin complexes, and shed further light on the information they can yield but equally on their (dis) advantages and limits.

All proteins absorb UV light in the range of 190–240 nm (peptide bond) and some with aromatic residues absorb around 280 nm. Aromatic rings in proteins also lead to intrinsic fluorescence emission (emission wavelength from 300 to 350 nm), which is highly dependent upon polarity and/or local environment. However, changes in intrinsic fluorescence due to protein/protein interactions are generally small, as they implicate only those aromatics directly involved in the interface, and are hence not easy to analyze. One strategy to eliminate this problem is to use a fluorophore with unique absorption or emission characteristics to label one partner, and to use changes in the fluorescence of this label to detect binding. Other physicochemical properties can be used to differentiate between bound and free proteins. In this chapter, we will focus our study on analytical ultracentrifugation (AUC), isothermal titration calorimetry (ITC), nuclear magnetic resonance (NMR), three powerful and complementary techniques in the field of MAP–MT interactions. We will also briefly discuss a spectrometric fluorescence or Förster resonance energy transfer (FRET) approach and co-sedimentation.

AUC supplies useful information on the size and shape of macromolecules in solution with very few constraints on the sample or the nature of the solvent. Some of the thermodynamic parameters measured by AUC include the molecular weight, association state, and equilibrium constants for reversibly interacting systems. Moreover, for samples containing many components or aggregates as well as high concentration samples, size distributions and average quantities may be measured and characterized. This tool is particularly suited for the study of tubulin and its partners, and comes as a valuable complement to electron microscopy. Since all MAPs change the assembly state of tubulin, AUC is usually the first step when studying a new MAP–tubulin binding reaction. From AUC, two complementary views of macromolecules in solution behavior are accessible: (1) sedimentation velocity gives essential hydrodynamic information about the size and shape of molecules and (2) sedimentation equilibrium provides extra thermodynamic knowledge about the solution molar masses, stoichiometry, and association constants. For all these reasons, AUC is one of the most useful and well-established technique widely used in the field of tubulin biochemistry. Indeed, AUC was extensively used

with tubulin and was responsible for major breakthroughs concerning the formation of the tubulin network. In the beginning of the seventies, the polymorphism of polymerization and depolymerization of microtubules has been largely exemplified by the pioneers' work of Borisy (Borisy *et al.*, 1972). Using the famous "Beckman Model E," they extensively characterized the equilibrium between a 6S tubulin dimer species and 20–30S oligomers species (Borisy *et al.*, 1972; Marcum and Borisy, 1978; Scheele and Borisy, 1978; Vallee and Borisy, 1978). At the end of these studies it was finally concluded that the formation of oligomeric species was promoted by high molecular weight proteins, which turned out to be what we now call MAPs. In 1974, Frigon *et al.*, using electron microscopy and AUC, observed with pure tubulin in presence of magnesium ion that the 6S tubulin dimer peak was in equilibrium with a 36S faster peak constituted of ring tubulin oligomers (Frigon *et al.*, 1974). Then, Frigon and Timasheff, in two major publications, fully characterized the molecular mechanism of magnesium ion induced self-association of pure tubulin (Frigon and Timasheff, 1975a,b). The role of GDP in the self-assembly of tubulin into various structures was probed by sedimentation velocity (Howard and Timasheff, 1986). Later, in the eighties, Timasheff's group used AUC to study the ligand binding linked to tubulin self-association. The technique was also particularly successful in the study of the binding of the vinca alkaloids (vinblastine, vincristine, catharanthine) to tubulin (Na and Timasheff, 1980a,b; Na and Timasheff, 1986a,b). It was further developed in Correia's team, who analyzed thermodynamic data from many vinca alcaloid and analogues: from classical family members such as vinorelbine and vinflunine to new compounds such as eribulin (Alday and Correia, 2009; Chatterjee *et al.*, 2001; Lobert and Correia, 2007; Lobert *et al.*, 1998).

In our laboratory, we used AUC to address the question of the oligomerization state of HSP90 (Garnier *et al.*, 2002) as well as the interaction between cytochrome C3 type I and II (Pieulle *et al.*, 2005), but most of all, we used it to study tubulin. We analyzed the ring formation process after C-terminal cleavage of both α and β tubulin chains by subtilisin (Peyrot *et al.*, 1990; Peyrot *et al.*, 1991) as well as ring formation induced by cryptophycin 52 (Barbier *et al.*, 2001). Lately we have been applying AUC to the interaction between tau and microtubules (Devred *et al.*, 2004) and also, along with microcalorimetry techniques, on stathmin–tubulin interactions (Devred *et al.*, 2008) as we will discuss in the last section.

Once the oligomeric states of tubulin/MAP complexes are known, other methods can be used for the full characterization of their interaction. A full thermodynamic characterization of a binding reaction means the determination of the free energy change, ΔG, the enthalpy change, ΔH, and the entropy change, ΔS. ΔH and K_a are measured or fitted to experimental data, and ΔG and ΔS, can be easily calculated from ΔH and K_a using the following relationships:

$$\Delta G = -RT \ln K_a \tag{1}$$

$$\Delta H = -R \frac{\mathrm{d}(\ln K_a)}{\mathrm{d}(1/T)} \tag{2}$$

$$\Delta S = R \frac{\mathrm{d}(\ln K_a)}{\mathrm{d}(\ln T)} = \frac{\Delta H - \Delta G}{T} \tag{3}$$

It is also valuable, as we will see, to measure the change in heat capacity at constant pressure,

$$\Delta C_{\mathrm{p}} = \left(\frac{\mathrm{d}\Delta H}{\mathrm{d}T}\right) \tag{4}$$

In fact, ΔH is best measured directly by calorimetry. Microcalorimetry, based on the exchanges of heat accompanying the interaction between two (macro)molecules, was first described as a method for the simultaneous determination of binding constant (K_{a}) and enthalpy variation (ΔH), 40 years ago (Christensen *et al.*, 1966). A calorimeter measures the heat taken up from the environment (endothermic process) or heat given up to the environment (exothermic process). In contrast to spectroscopic methods, calorimetric measurements can be used to measure the interaction between molecules that are "spectroscopically silent" (no chromophore nor fluorophore tag is required), or in buffer conditions that would render spectroscopic measurement difficult to interpret (turbid, opaque, UV absorbing or heterogeneous solutions).

Over time, our laboratory has gained considerable experience with ITC to characterize the thermodynamics of various protein/ligand complexes. As examples, we measured the thermodynamic parameters of the interaction between: cephalosporins and human serum albumin (Briand *et al.*, 1982); methotrexate and some of its metabolites with dihydrofolate reductase (Gilli *et al.*, 1988) and thymidylate synthase (Gilli *et al.*, 1990); Ca^{2+}, Mg^{2+}, and calmodulin (Gilli *et al.*, 1998); coumarins and gyrase fragment (Lafitte *et al.*, 2002); vinca alkaloid and calmodulin (Makarov *et al.*, 2007).

Recently this technique has been used to characterize the binding of stathmin to tubulin (Honnappa *et al.*, 2003). We thus used it to study the influence of antimitotic drugs on the binding of stathmin to tubulin. ITC enabled us to show that vinblastine significantly increases stathmin affinity for tubulin and that stathmin has the same effect on the vinblastine binding constant for tubulin (Devred *et al.*, 2008). ITC is a very powerful tool to obtain a quick and reliable comparison of the thermodynamic parameters of interaction of two molecules in solution, but it does not give any information on the nature of the species in solution. This is why it is usually coupled to AUC or electron microscopy.

Beside ITC and AUC, one of the most commonly used indirect binding methods is the change of the ligand fluorescence on binding and the quenching of the intrinsic protein fluorescence. Let us recall that data interpretation of spectral methods typically depends on *a priori* assumptions that there is a correlation between the spectral changes and the amount of the ligand bound (Bujalowski and Lohman, 1987). The chief assumptions are that the binding of each molecule of ligand induces an identical spectral change in the protein and that the degree of change in the spectral property varies linearly with the degree of saturation. Keeping in mind these assumptions, we largely used this method in the study of the binding of various ligands to tubulin (Barbier *et al.*, 1995; Barbier *et al.*, 1996; Leynadier *et al.*, 1993; Peyrot *et al.*, 1992; Rappl *et al.*, 2006).

In fluorescence, another important process that occurs in the excited state is resonance energy transfer. This process occurs whenever the emission spectrum of a fluorophore, called the donor, overlaps with the absorption spectrum of another

compound, called the acceptor (Förster, 1948). The acceptor does not need to be fluorescent. FRET occurs without the transfer of a photon, but rather is the result of long-range dipole–dipole interactions between the donor and acceptor. The distance dependence of FRET has resulted in its widespread use to calculate distances between donors and acceptors. For tubulin, intrinsic and extrinsic fluorescent probes have been used in conjunction with FRET methodologies to measure distances between different tubulin ligands (Bhattacharyya *et al.*, 1993; Bhattacharya *et al.*, 1996; Han *et al.*, 1998; Ward and Timasheff, 1988; Ward *et al.*, 1994), to monitor tubulin conformational changes (Bhattacharya *et al.*, 1994; Prasad *et al.*, 1986; Soto *et al.*, 1996), and to follow tubulin polymerization (Bonne *et al.*, 1985; Kung and Reed, 1989). For example, Ward *et al.* (1994) measured, by FRET experiments, the spatial separation between the colchicine and Ruthenium Red binding sites, the high-affinity bisANS and Ruthenium Red sites, and the allocolchicine and high-affinity bisANS sites on tubulin. Recently, Makrides *et al.* (2004) established a probe based on FRET that allowed measurement of the interaction between tau and microtubules. Tau does not contain any tryptophan residue (Trp), but does contain two cysteine residues (Cys-291 and Cys-322) that can be labeled to stoichiometry by the fluorophore acrylodan. This latter fluorophore then serves as an efficient acceptor of energy transfer from the tubulin donor tryptophan residues at the condition that the complex is formed. It should however be noted that the Trp/acrylodan pair is not a very efficient FRET pair, so this technique did not allow us to study the lower affinity accumulation of tau on MT surface as we will explain later.

NMR spectroscopy (see Chapter 22 by Clément *et al.*, this volume), although capable of providing structural and dynamic information on a per-residue basis in smaller systems, seems at first not ideally suited for the study of a macromolecular assembly comprising tau and tubulin. First, the size of the tubulin dimer, with a molecular weight of ~100 kDa, and outpassing the megadalton or higher when assembled in rings or microtubules, invariably leads to significant line broadening. Modern NMR techniques that exploit spin dynamics to reduce the transverse relaxation even in larger systems do crucially depend on deuteration of most of the carbons of the protein. The absence of an effective over-expression system for tubulin precludes this, and direct NMR analysis of tubulin therefore is currently out of reach. Tau, on the other hand, suffers from the fact that it is natively unfolded, and therefore shows a very limited dispersion of its amide proton resonances. Whereas this has proven to be a barrier for NMR analysis of this protein, despite its important physiological and pathological role, we realized that it also could be an advantage as it implies that the carbon chemical shifts of the residues are known (Lippens *et al.*, 2004). Based on this *a priori* knowledge, we could assign about 40% of the resonances, and very recently, Mukrasch *et al.* (2009) exploited the resolving power of a 900 MHz NMR spectrometer to obtain the full assignment of tau. However, our initial assignments proved to be largely sufficient for the study of molecular interactions (Sibille *et al.*, 2006) and for the effect of posttranslational modifications (Amniai *et al.*, 2009; Landrieu *et al.*, 2006). As for this latter aspect of evaluating the phosphorylation status of a complex sample as a multi-phosphorylated tau, NMR has some decisive advantages over other analytical techniques such as mass spectrometry and/or immunochemistry. Although it requires at least ^{15}N-labeling of the protein, and can therefore not be performed on material isolated from brain or other tissues, NMR allows us to see all the sites that are modified in a

single experiment, and can readily identify and quantify them. This later aspect is important, as even the notion of "hyperphosphorylated" often used in the literature to characterize PHF-tau has not yet been properly defined.

Here, we would like to address the feasibility of using NMR to study MAP–MT complexes, taking into account several experimental considerations. First, tau decreases the critical concentration for tubulin assembly into microtubules at 37°C. At lower temperature, tau promotes the formation of rings, and therefore significantly increases both the size and the heterogeneity of the sample. Measuring directly at 37°C is also problematic, as the amide protons of tau exchange rapidly with water protons, leading to broader lines when working at higher temperatures. Second, when working directly with taxol-stabilized MTs, two limiting factors are the inherent instability of tubulin (even with the best purification protocol, samples are rarely stable after 24 h) and the limit imposed on the concentration as microtubules tend to form a liquid crystalline phase above a critical concentration (Hitt *et al.*, 1990). The third consideration concerns the stoichiometry of tau on the tubulin surface. Whereas accumulation of tau on the MT surface has been described from the early eighties on (where it was called "the parking problem"), and can be reproduced by the co-sedimentation experiments we described above, the stoichiometry as determined by fluorescence (Makrides *et al.*, 2004) seems to be one tau molecule per two tubulin heterodimers. Taken together, these factors limit the nature of the NMR experiments that are feasible, especially when considering the inherent poor sensitivity of NMR. Still, we want to show in the present review that NMR experiments on the isolated MAPs can be extended to their complexes with different forms, and that these *in vitro* studies can complement the above-described experiments that give further insight in the thermodynamic parameters derived.

Valuable information about the molecular mechanisms that govern the highly dynamic yet tightly regulated MT–MAP system can be obtained by studying the thermodynamics of complex formation between the cytoskeleton network and its regulators. We will present in this chapter how biophysical techniques such as AUC, ITC, FRET, NMR, and co-sedimentation can be applied to MAPs focusing on tau and stathmin and what precautions must be taken while applying them to such a delicate system as MT cytoskeleton, each technique having its advantages, qualities, requirements, and limits.

III. Materials and Methods

A. Protein Purification and Sample Preparation

Tubulin extraction from lamb brain was conducted following the Weisenberg procedure well described in microtubule protocols (Andreu, 2007). Tau and stathmin were recombinant proteins. Human hTau40 (the largest tau isoform) and stathmin were expressed from a pET vector introduced into *Escherichia coli* BL21(DE3). Expression was induced by isopropyl 1-thio-D-galactopyranoside (IPTG) during the bacterial exponential growth phase. Tau bacterial lysates obtained by sonication, were heated at 90°C. After being cleared by centrifugation at 17,000 × *g* for 20 min at 4°C, the supernatant was loaded onto a 5 ml HiTrap™ SP Sepharose HP cation exchange column (GE Healthcare) pre-equilibrated with 50 mM MES (pH 6.5) and

eluted with a buffer consisting of 50 mM MES and 0.5 M NaCl (pH 6.5). Fractions containing tau protein were pooled, dialyzed overnight against 50 mM ammonium bicarbonate and dry-lyophilized. Stathmin purification was also realized without the use of tag that might modify its structural physical and interacting properties., Since stathmin is thermostable like tau, the preparation was boiled and then purified using an anion exchange column 5 ml Hitrap^{TM} DEAE-FF. An additional reverse phase step (15RPC PE 7.5/150) was then used to get rid of the degraded form of stathmin (Devred *et al.*, 2008). Fractions containing stathmin were pooled and directly dry-lyophilized. Purity was evaluated by SDS-PAGE and then confirmed by MALDI mass spectrometry and peptide mass fingerprinting.

Tubulin concentration was determined spectrophotometrically at 275 nm with an extinction coefficient of 109,000 M^{-1} cm^{-1} in denaturizing conditions (6 M guanidine hydrochloride). The concentration of tau, which has an extinction coefficient 7700 M^{-1} cm^{-1} at 280 nm, was determined using its absorbance spectrum (220–450 nm) corrected for light scattering. Since stathmin bears no aromatic residues, we used colorimetric methods (DC Protein Assay, Biorad) with BSA as standards.

For microcalorimetry and AUC methods, it is extremely important to use identical buffers for references and sample solutions. For ITC especially, due to the extreme sensitivity in the signal measurement, it is extremely important that the two solutions be matched with regard to composition, pH, buffer, and salt concentration. If the two solutions are not perfectly matched, there may be heat of mixing (or dilution) signals that will overwhelm the heat signals for the binding reaction. After purification, tubulin is stored in buffer containing 1 M sucrose to stabilize its conformation and is stable for several years when stored in liquid nitrogen. Before tubulin is used the sucrose should be removed. For most of the systems, extensive dialysis is usually employed to exchange buffers. Nevertheless, because of tubulin fragility it is not possible to dialyze it in absence of a stabilizer such as sucrose. Tubulin was thus passed through a drained gel filtration Sephadex G25 resin equilibrated with appropriate buffer using a spin column (1 × 5 cm), followed by a passage through second larger (1 × 10 cm) gravity column packed with Sephadex G25 resin equilibrated with the same buffer (Barbier *et al.*, 1998; Peyrot *et al.*, 1992). Dry lyophilized tau and stathmin were directly dissolved in the desired buffer just before use, to minimize the possible heat of mixing in ITC. After centrifugation to remove the aggregated proteins, the concentration was measured (see above).

To phosphorylate recombinant tau protein, tau (10 μM) was incubated with 0.1 μM recombinant PKA catalytic subunit (for the PKA phospho-Tau) or with 0.08 μM of the recombinant cyclin-dependent kinase CDK2/CycA3 in a buffer containing 1 mM ATP, 12.5 mM $MgCl_2$, 50 mM HEPES (pH 8), 55 mM NaCl, 5 mM DTT, and 1 mM EDTA for 16 h at 20°C. The reaction mixture was then buffer exchanged against 50 mM ammonium bicarbonate before lyophilization. SDS-PAGE (12%) was used to check the integrity of the samples. Tau incubated in the kinase buffer without kinase or without ATP was used as control in the polymerization experiments.

B. Analytical Ultracentrifugation

AUC consists of the application of a centrifugal force that induces sedimentation of a macromolecule or a mixture of macromolecule in solution. This sedimentation is observed by detection of the macromolecule during the centrifugation by absorbance

or interference optics. As already mentioned the sedimentation of a macromolecule is linked to its shape and molecular weight by the following relation:

$$S = \frac{M(1 - v\rho)}{Nf} \tag{5}$$

With S the sedimentation coefficient in Svedberg (10^{-13} s), M the molar mass, v the partial specific volume, f the frictional coefficient of the macromolecule, ρ the solvent density, and N the Avogadro number. Sedimentation velocity data can be analyzed by different software available on the http://www.bbri.org/RASMB/rasmb.html web page. Some of them, such as Sedfit program developed by P. Schuck, were based on the analysis of the detailed sedimentation-diffusion equation, the Lamm equation, which describes the evolution of the complete concentration profiles during sedimentation velocity run ($C(S)$ distribution). Other, such as DCDT+™ program developed by J. Philo, implements the time derivative data analysis (dc/dt methods) originally developed by W. Stafford; for details see (Scott and Schuck, 2005). We will use these two approaches to quantify the interaction between tau/stathmin and tubulin by AUC. Partial specific volume of tau and stathmin are 0.724 and 0.7341 ml/g respectively, both predicted by the software SEDNTERP (Laue *et al.*, 1992) and that of tubulin is 0.736 ml/g (Lee and Timasheff, 1974) at 20°C. The buffer used in all experiments was phosphate buffer 20 mM, GTP 10 μM, pH 6.5 and its density and viscosity were 1.009 g/ml and 0.001047 poise, respectively. Tubulin needs GTP in the buffer to stabilize its conformation over the time range of centrifugation. More generally, 0.1–1 mM of GTP is employed but nucleotides absorb in the UV protein range and the UV scans are consequently noisy within this range of nucleotide concentration. Thus, for sedimentation velocity experiments involving tubulin, we used minimum GTP concentration, i.e., 10 μM. Under these conditions the nucleotide composition of tubulin was 87% GTP–tubulin, which is not significantly different from the 90% GTP–tubulin equilibrated with 10^{-4} M GTP (Devred *et al.*, 2004). Various concentrations of protein or protein mixtures were run at 40,000 rpm at 20°C in a Beckman Optima XL-A analytical ultracentrifuge equipped with absorbance optics, using 12 mm charcoal filled Epon double-sector centerpieces and tubulin concentrations as low as 2 μM. Data were acquired in continuous mode at 280 nm or 290 nm. For tau characterization, higher speed was used (55,000 rpm) with a 12 mm aluminum double-sector centerpiece.

C. Co-sedimentation Assay

In addition to ITC and AUC, co-sedimentation assay can be used for affinity constant determination by assessing the amount of bound and free ligand and receptor. In this part, we will focus on tau–tubulin interaction. Taxol-stabilized MTs were formed by incubation of 15 μM of tubulin with 15 μM of taxol during 25 min at 37°C in phosphate buffer 25 mM, NaCl 25 mM, pH 7 with 8 mM $MgCl_2$, DTT 0.4 mM, GTP 0.1 mM. In this buffer, NaCl is used to avoid nonspecific electrostatics interactions, DTT to maintain tau in its monomeric forms and magnesium is indispensable for taxol-induced MT formation. The stabilized microtubule solutions (200 μl) were then diluted to the desired concentration (5 μM), taxol added to maintain a tubulin/taxol molar ratio of about 1.5 and titrated with different

concentrations of tau (from 2.5 to 20 μM). The 200 μl samples were deposed on a 200 μl layer of 60% glycerol, diluted in the same buffer, to eliminate nonspecific binding during the centrifugation. After 20 min of centrifugation at 88,000 × *g* at 20°C (Beckman TL-100, rotor TL 100.2), the concentrations of tau in the pellets (bound tau) and the supernatants (free tau) were determined by densitometry on SDS-PAGE with tubulin concentration as standard. Pellets and corresponding supernatants should be loaded in the same SDS-PAGE to eliminate error due to variation in coloration. Because both free and bound tau concentrations were available, we can use a Scatchard representation to determine the affinity constant and the stoichiometry of the reaction. The Scatchard equation is given by $B/[F] = nK_a – BK_a$ where B is the ratio of the concentration of bound ligand (here tau in the pellet) to total available binding sites (total tubulin concentration), $[F]$ is the concentration of free ligand, n is the number of binding sites, and K_a the affinity constant of tau for the microtubule. Plotting this data, $B/[F]$ versus B, yields the Scatchard plot with a slope $–K_a$ and an x-intercept of n.

This approach was also used to find the nature of the ligand-induced macromolecular self-association in the case of tau-induced tubulin self-association into microtubules. In that case, Scatchard plots are usually curved downward reflecting the fact that ligand-induced tubulin assembly may proceed by two different pathways (Devred *et al.*, 2004): either a ligand-facilitated elongation pathway, in which the elongation precedes the binding of the ligand (Eq. 6) or a ligand-mediated elongation pathway, in which the binding of tau, to either tubulin or microtubule, precedes the elongation (Eqs. 7 and 8).

$$\mathrm{MT} + \mathrm{Tub} \overset{K_2}{\longleftrightarrow} \mathrm{MT} - \mathrm{Tub} + \mathrm{tau} \overset{K_1}{\longleftrightarrow} \mathrm{MT} - \mathrm{Tub} - \mathrm{tau} \tag{6}$$

$$\mathrm{tau} + \mathrm{Tub} \overset{K_1}{\longleftrightarrow} \mathrm{Tub} - \mathrm{tau} + \mathrm{MT} \overset{K_2}{\longleftrightarrow} \mathrm{MT} - \mathrm{Tub} - \mathrm{tau} \tag{7}$$

$$\mathrm{MT} + \mathrm{tau} \overset{K_1}{\longleftrightarrow} \mathrm{MT} - \mathrm{tau} + \mathrm{Tub} \overset{K_2}{\longleftrightarrow} \mathrm{MT} - \mathrm{Tub} - \mathrm{tau} \tag{8}$$

Equation (6) is characterized by an apparent elongation constant $K_{app} = K_2(1 + K_1[\mathrm{tau}])$. Equations (7) and (8) are not thermodynamically discernible and are characterized by an apparent elongation constant $K_{app} = K_1K_2[\mathrm{tau}]/(1 + K_1[\mathrm{tau}])$ (for more details, see the appendix of Buey *et al.*, 2004). The equation best fitting the data, using a graphics fitting program (Sigmaplot 4.0, Jandel Scientific), will favor one or the other model.

D. Fluorescence or Förster Energy Transfer (FRET)

FRET was extensively employed to measure distance between different reactive sites in a protein, proteins in lipids or in cell surface. With recent advances in fluorescence microscopy, it has also been used to study direct protein–protein interaction in living cells and in solution. While the fluorescence methods seem quite simple and sensitive, special care must be taken to study the interaction between two proteins (Garnier *et al.*, 1998). Indeed, fluorescence requires proper spectral corrections for a number of possible artifacts: light scattering, inner filter effects, and temperature dependence of fluorescence quantum yields. These

problems are particularly important in the determination of the maximal spectral perturbation needed to establish the extent of binding. In FRET, a donor molecule with a fluorophore absorbs light at a certain wavelength to be in a higher electronic energetic state. Then, the acceptor in the proper orientation and distance receives a nonradiative transfer of energy from this donor, resulting from a dipole–induced dipole interaction. If the acceptor molecule is fluorescent, it is then excited to a higher electronic energetic state and electrons decay back down emitting fluorescence photon at larger wavelength (stoke shift). There are three conditions necessary for efficient energy transfer: the donor emission spectrum must overlap the acceptor absorbance spectrum, the donor and acceptor fluorophores must be sufficiently aligned so that an acceptor dipole can be induced by the donor, and the donor must not be separated from the acceptor by a distance greater than ~60 Å.

For tau–tubulin interaction we used acrylodan (6-acryloyl-2-dimethylaminonaphthalene)-labeled tau to study the tau–tubulin interaction, with the fluorophore covalently attached to Cys-291 and Cys-322 (Makrides *et al.*, 2004). To label the protein, tau was first extensively reduced with a 10-fold molar excess of DTT for 2 h, desalted on a 5 ml column of sephadex G-25 to remove the excess of DTT and then incubated 2 h in a dark room with a 10-fold molar excess of the thiol reactive acrylodan. Unincorporated acrylodan was removed by a size exclusion chromatography Sephadex G25. To avoid problems in protein concentration determination that could arise from the absorption of the residual fluorophore, ^{15}N-labeled tau was used for this fluorophore labeling, allowing accurate determination of its concentration by comparison of its signal intensity in a 1D ^{1}H-^{15}N HSQC spectrum with that of a reference spectrum obtained from a ^{15}N-labeled sample before acrylodan labeling. 1 μM of MTs solution was mixed with various tau–acrylodan concentrations. Fluorescence spectra are recorded from 460 to 540 nm with an excitation wavelength of 290 nm. Similar measurements were also done without microtubules. Fluorescence signal caused by FRET was taken as the difference between the fluorescence intensity emitted from labeled-tau in the presence versus the absence of microtubules, at the emission wavelength giving the maximum fluorescence. This fluorescence corrected signal was plotted versus total tau-labeled concentration and fitted with the following equation:

$$F = F_{\max}\,(b - \sqrt{b^2 - 4ac})/2a + y \tag{9}$$

where F is the experimental fluorescence emission intensity at 490 nm; c the acrylodan–tau concentration, $F_{\max}$ the fluorescence at saturating tau levels, a is the concentration of tau binding sites, $b = a + c + K_d$, and y is the y-intercept value. The maximal stoichiometry of binding, n, was derived from $a = n \times$ tubulin concentration.

E. Microcalorimetry (ITC)

Almost any chemical reaction or physical change is accompanied by a heat change. ITC is a thermodynamic technique that allows the study of interactions between molecules by measuring the heat released or absorbed by interacting molecules. Since heat exchange upon binding occurs naturally, ITC does not require

immobilization and/or modification of the reactants. Thermodynamic characteristics such as binding constants ($\sim 10^3 - 10^8\ M^{-1}$) and reaction stoichiometry can be determined from the measurements. Given improvements in ITC instrumentation and data analysis software, it is now routinely used to directly characterize the thermodynamics of binding interactions in many systems (Freire *et al.*, 1990). Heat measurements can be made in different ways, such as temperature change (adiabatic) or power compensation (isothermal) principles; see review (Freyer and Lewis, 2008). Here we used ITC to directly measure the heat of reaction, i.e., the enthalpy variation of the reaction ΔH. The reaction takes place in a compartment in which ligand is injected using a syringe. In that system, the temperature of the calorimeter measurement cell is maintained constant (isothermal), by means of a temperature controller. As a chemical reaction takes place in the cell, any heat change is sensed and the appropriate electric power is applied to the controller so that again the temperature remains constant. The heating power from the two sources, reaction and controller, are kept at a constant level so that a heat input from the reaction is compensated by a drop in the heat input from the controlled heater. The raw signal in the power compensation calorimeter is the power (mcal/s or mJ/s) applied to the controller that is required to keep the calorimeter cell from changing temperature as a function of time. A measure of the heat given to or taken from the buffer, for exothermic or endothermic processes respectively, is proportional to the number of moles that reacted and to the enthalpy change for the reaction, ΔH (kcal/mol or kJ/mol). The heat change is then simply calculated by integrating the heater power over the time (s) required for the controller power to return to a baseline value.

The thermogram generated in the ITC experiment is a simple summation of all of the heat-producing reactions that occur as an aliquot of titrant is added. In the case of one or several identical binding site, the initial heat peaks are larger than the heat peaks for subsequent additions, since at the beginning of the titration there is a large excess of empty or unpopulated binding sites. Initial heat peaks most typically are the result of complete reaction of the added ligand. As the titration proceeds, less and less of the added ligand is bound and there are three species existing in solution: free ligand, free protein binding sites, and the ligand–protein complex. The heat produced in the ITC experiment is linearly dependent on the ΔH of the reaction and non-linearly dependent on the K. The goal is to model the experimental data within expected experimental error, using the simplest model, in light of what is already known about the system (e.g., stoichiometry).

In our hands, tubulin concentration was set in the 5–20 μM range in the cell whereas stathmin or tau was in the 15–50 μM range. Practically, in the case of a microcalorimetry system with ITC unit (MCS-ITC), which can theoretically operate between 0 and 80°C, 2.5 ml of tubulin sample need to be prepared to fill the 1.4 ml cell, and a minimum of 750 μl of ligand (tau or stathmin) to fill the injection syringe. The next generation model VP ITC, though more sensitive and with Peltier-controlled rapid temperature equilibration, had about the same volume requirements. The newest model of Microcal, iTC200, has drastically improved the two limiting factors: time and quantities. With this new apparatus, experiments require 300 μl to fill the sample cell and 70 μl to fill the injection syringe. With fast equilibration times, up to two runs per hour can be easily accomplished. Furthermore iTC200 will soon be upgraded to a fully automated version with a sample throughput of at least 50 samples per day.

Despite of all the precautions taken to match buffer in the syringe and in the cell (see above) there might still be some heat due to the dilution of the ligand itself and even sometimes of the tubulin in the cell. To take these factors into considerations two controls are to be performed. In a first one, the ligand solution is titrated into buffer in the sample cell. In a second one, the heat of dilution of tubulin will also be measured by simply injecting buffer from the syringe into the tubulin solution in the sample cell. Usually the heat of dilution of the macromolecule measured in this way is negligible. Furthermore, since the generation of bubbles in the sample solutions during an ITC experiment will disturb the detection of the heat exchange due to the binding, the solutions should be degassed prior to filling the cell and injection syringe.

Another calorimetric reaction that might occur in parallel of the measured binding is the exchange of protons between the interacting molecules and the buffer, as binding occurs. Indeed, to facilitate binding, residues at the interface may be protonated or deprotonated, resulting in exchange of protons with the buffer. Calorimetry measures the totality of heat effects in any process, and therefore detects protonation changes involved in ligand binding as well. Although the enthalpic contributions of protein conformational changes can be taken as an integral component of the overall binding process, the enthalpy contribution due to protonation–deprotonation of the buffer species must be subtracted from the enthalpy change observed to obtain the binding enthalpy of the complex formed. To overcome this problem and therefore obtain the true enthalpy of interaction, ITC titrations have to be performed in buffers with significant differences in heat of ionization. For example experiments can be performed successively in Tris–HCl (47.4 kJ/mol) and Hepes (20.5 kJ/mol). The analysis of the dependence of the experimental ΔH observed in the various buffers (ΔH_{obs}) will provide the number of proton exchanged during the binding process and the true enthalpy of binding. Another option is, when possible, to perform experiments in buffers with a small heat of ionization such as phosphate buffer (~5.0 kJ/mol).

F. NMR Spectroscopy Involving Tubulin

As NMR experiments on a protein of the size of tubulin absolutely require deuteration to limit relaxation, the present impossibility of recombinant production of tubulin make direct NMR observation of anything except the most flexible polyglutamate tails nearly impossible. The purification protocols from animal tissue, although well optimized and leading to substantial amounts of material, come with a limited stability of the purified protein, thus limiting the applicability of the insensitive NMR technique. Finally, when working with microtubules, the concentration of the solution is equally restricted, as MTs tend to form an ordered phase in solution above a critical concentration of 38 μM (Hitt *et al.*, 1990). Adding to this is the possible accumulation of tau on the MT surface, making it necessary to work at substoichiometry ratios to probe the true tau:MT binding. Thus, the window of experimental conditions in which to probe the tau:MT interaction by NMR spectroscopy becomes rather narrow. The binding partners of tubulin, be it tau or stathmin, can however be recombinantly produced, and hence labeled with the required stable isotopes. In our first attempts, we used ^{15}N-labeled tau and a 1:4 ratio of tau:tubulin dimer to avoid the previously mentioned stacking problem. NMR spectra were acquired overnight on a 600 MHz spectrometer equipped with a cryogenic probe

head, which proved sufficient to detect those parts of tau not implicated in the binding at the MT surface. It should be stressed that the experiment with only 5 μM of tau succeeded because of the narrow line width of tau due to its natively unfolded character. For a folded protein of similar size, we would not expect to obtain a reasonable spectrum without extensive deuteration and transverse relaxation optimized spectroscopy (TROSY) (Pervushin *et al.*, 1997) at the highest fields available.

IV. Discussion

Three different issues can be addressed by our techniques. First, detecting MAP binding to tubulin and characterizing the complexes formed; this part will be restricted to the use of AUC to characterize tau-induced rings and stathmin-induced T2S complex formation (this is detailed in Chapter 15 by Correia, this volume). Second, we will focus on determining the thermodynamic parameters of the binding of the MAP to tubulin or MT. This part will address the use of a co-sedimentation assay with taxol-stabilized MT, FRET to characterize tau binding to MTs, and the use of ITC to characterize stathmin binding to tubulin in absence and in presence of antimitotic drugs. Third, we will present how NMR can help us to identify which amino acids of tau are implicated in its binding to MTs. This will also be used in the study of the role of specific phosphorylation of tau.

A. Evidences of MAP–Tubulin and Microtubules Complexes Formation

As already mentioned, AUC has been extensively used to study the oligomeric state of tubulin induced by small molecules such as magnesium or the vinca alkaloids family and provides an accurate tool for the study of MAP–tubulin interaction. In this part, we will discuss how to study a protein–protein interaction by sedimentation velocity taking the tau–MT and stathmin–tubulin interactions as examples. In order to study the interaction of two proteins by sedimentation velocity, it is first necessary to determine the sedimentation coefficient of each partner independently in the experimental conditions. Figure 1A represents the sedimentation distribution $C(S)$ at two tubulin concentrations. This distribution shows one peak centered at an apparent sedimentation coefficient of 5.59 ± 0.08 and 5.54 ± 0.07 S for 0.9 and 1.2 mg/ml of tubulin respectively, confirming its monodisperse state. Since the experimentally observed sedimentation coefficient vary with temperature and solution density, we converted it into a standard state of 20°C in water ($S_{20,W}$) using SEDNTERP program (Laue *et al.*, 1992). We then plotted the $S_{20,W}$ versus various concentrations of tubulin to determine the standard sedimentation coefficient at 20°C in water at infinite dilution (inset of Fig. 1A) which is 5.97 ± 0.05 S. The frictional coefficient ratio (f/f_0), parameter reflecting the form of the molecule, could be calculated as $f/f_0 = S_{max}/S$ ratio where f_0 and S_{max} are the frictional and sedimentation coefficients of a smooth unhydrated sphere corresponding to the given protein mass, S is the experimental sedimentation coefficient obtained by AUC, and f is the frictional coefficient of the protein (Philo, 2000). The S_{max} was calculated by Sedfit and was 7.49 S giving a $f/f_0 = 7.49/5.97 = 1.25$. A similar approach was used for the second partner, i.e., tau. Tau is a natively unfolded protein of

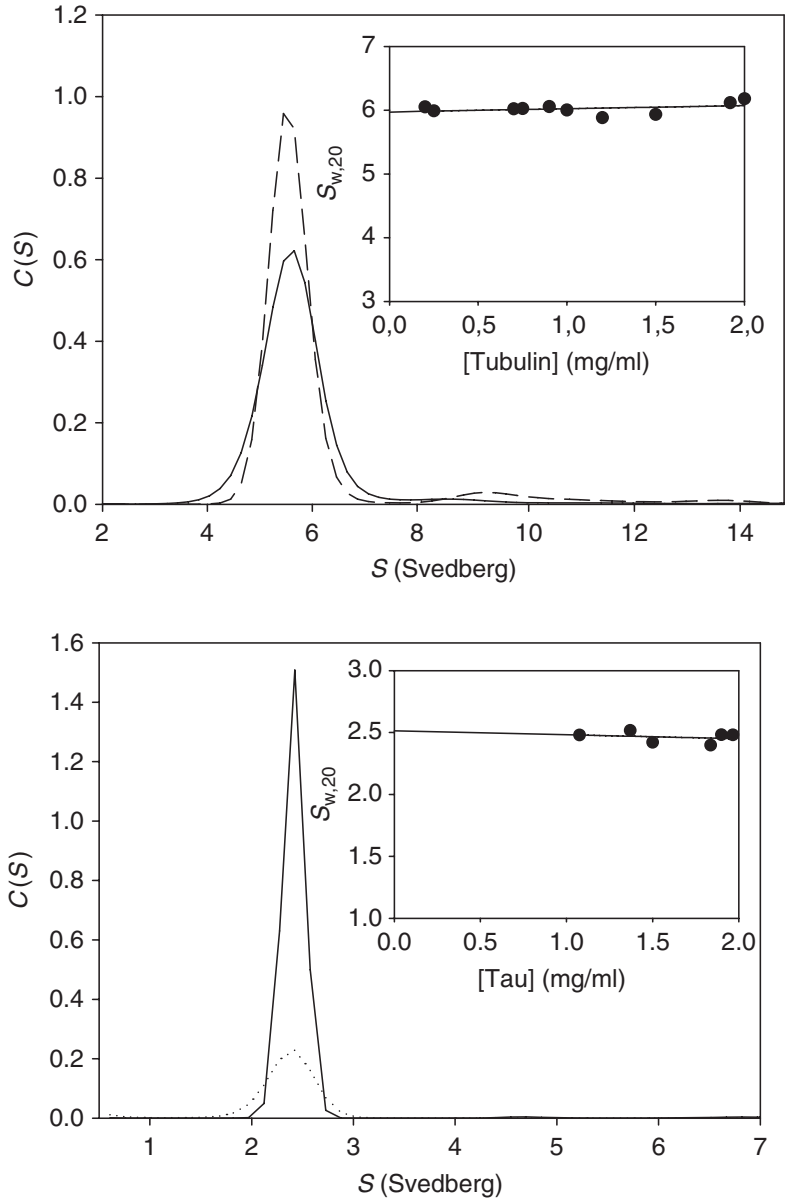

Fig. 1 (A) Sedimentation distribution of tubulin obtained by Sedfit program (1.2 mg/ml dark line and 0.9 mg/ml dashed line) at 20°C. Inset: determination of the standard sedimentation coefficient of 20°C in water at infinite dilution of tubulin. (B) Sedimentation distribution of tau obtained by Sedfit program (1.5 mg/ml dark line and 0.8 mg/ml dashed line) at 20°C. Inset: determination of the standard sedimentation coefficient of 20°C in water at infinite dilution of tau.

45,850 Da. Like tubulin, tau sedimentation is monodisperse (Fig. 1B) and the standard sedimentation coefficient of 20°C in water at infinite dilution (inset of Fig. 1B) is 2.5 ± 0.1 S. For tau, we calculated by Sedfit the theoretical sedimentation coefficient of a smooth anhydrate sphere corresponding to 45,850 Da, S_{max} that is 4.5 S and obtained a frictional coefficient ratio f/f_0 of 1.8 corresponding to a much-extended protein. We have characterized the two partners of the interaction, showing that both of them are monodisperse and have relatively different sedimentation coefficients. These two conditions are favorable to study their interaction analyzing the sedimentation profile of various mixture of the two

proteins monitored at 280 nm, or 290 nm for concentrated tubulin samples, keeping in mind that the sedimentation are not additive. Because tubulin is a protein containing eight tryptophane residues with an extinction coefficient at 280 nm of 116,000 M^{-1} cm^{-1} and tau, a protein containing only tyrosine with a 15-fold lower extinction coefficient ($\varepsilon_{280\,nm} = 7700\,M^{-1}\ cm^{-1}$), the absorbance signal contribution of tau could be neglected. Note that the difference in their extinction coefficient is more pronounced at 290 nm. It is important at this stage to discuss the choice of the data analysis. We know from the previous experiments with protein alone that tubulin and tau have very different frictional coefficient ratio. *C* (*S*) distribution assumes that all species present in the solution have a uniform frictional ratio, which is not clearly the case for tubulin and tau. Thus, we analyzed the data using the apparent sedimentation coefficient distribution $g(s^*)$ generated by DCDT+ program (Philo, 2000; Stafford, 1992). As expected for monodisperse species, tubulin and tau sedimentation profiles analyzed by DCDT+ are similar to that obtained by Sedfit. Figure 2A shows the single Gaussian distribution of $g(s^*)$ of 16 μM tau and 15 μM tubulin obtained in separate experiments. As with Sedfit, the tubulin peak was centered on 5.43 ± 0.03 S and the tau peak on 2.29 ± 0.08 S. Tubulin at fixed concentration was mixed with various concentrations of tau. The distributions $g(s^*)$ were then fitted with Gaussian curves, and the areas and maximum, which represent the sediment coefficient of the sample, were calculated. We used this analysis to qualitatively characterize the tau–tubulin interaction, keeping in mind that the boundaries do not represent individual species but interacting zones. Figure 2B shows a trimodal pattern resulting from the interaction of 15 μM tubulin and 7.5 μM tau. The $g(s^*)$ distribution, which is very sensitive to the presence of multiple species, was fitted with three Gaussian curves centered on 6S, 30–35S, and 40–50S, respectively. To test the nature of the equilibrium, similar experiments were performed at a 30,000 rpm. They led to the same sedimentation pattern, indicating that this self-associating system was in rapid equilibrium (Lee and Rajendran, 1994). Amount of the different sediment boundaries (inset of Fig. 2B) were calculated by integrating the Gaussian curves obtained for the different peaks for different tau/tubulin molar ratios and different tubulin concentrations and the results obtained indicated that the formation of these different species is an equilibrium system dependent on tubulin and tau concentration. To visualize the structure of the polymers formed, we used transmission electron microscopy. Complexes evidenced by AUC consisted of circular polymers that were mostly single wall rings with an average external diameter of about 45 ± 5 nm and an internal diameter of 30 ± 5 nm, corresponding to about 14 tubulin dimer rings and the presence of other circular polymers, such as thick wall rings and possibly spirals, as well as partial rings (Devred *et al.*, 2004). This structural heterogeneity could explain the wide profile of peaks in the $g(s^*)$ distribution of the fast sedimenting species in the sedimentation velocity experiment (Fig. 2B). Because of the numerous structures of tubulin oligomers in the presence of tau, only qualitative data could be obtained by AUC. However, this method is an immediate method to check tau binding and functionality (Amniai *et al.*, 2009). For example, we used it to study the effect of posttranslational modification of tau known to regulate its interaction with tubulin. By reporting the amount of the slower sedimenting peak as a function of tau/tubulin ratio we

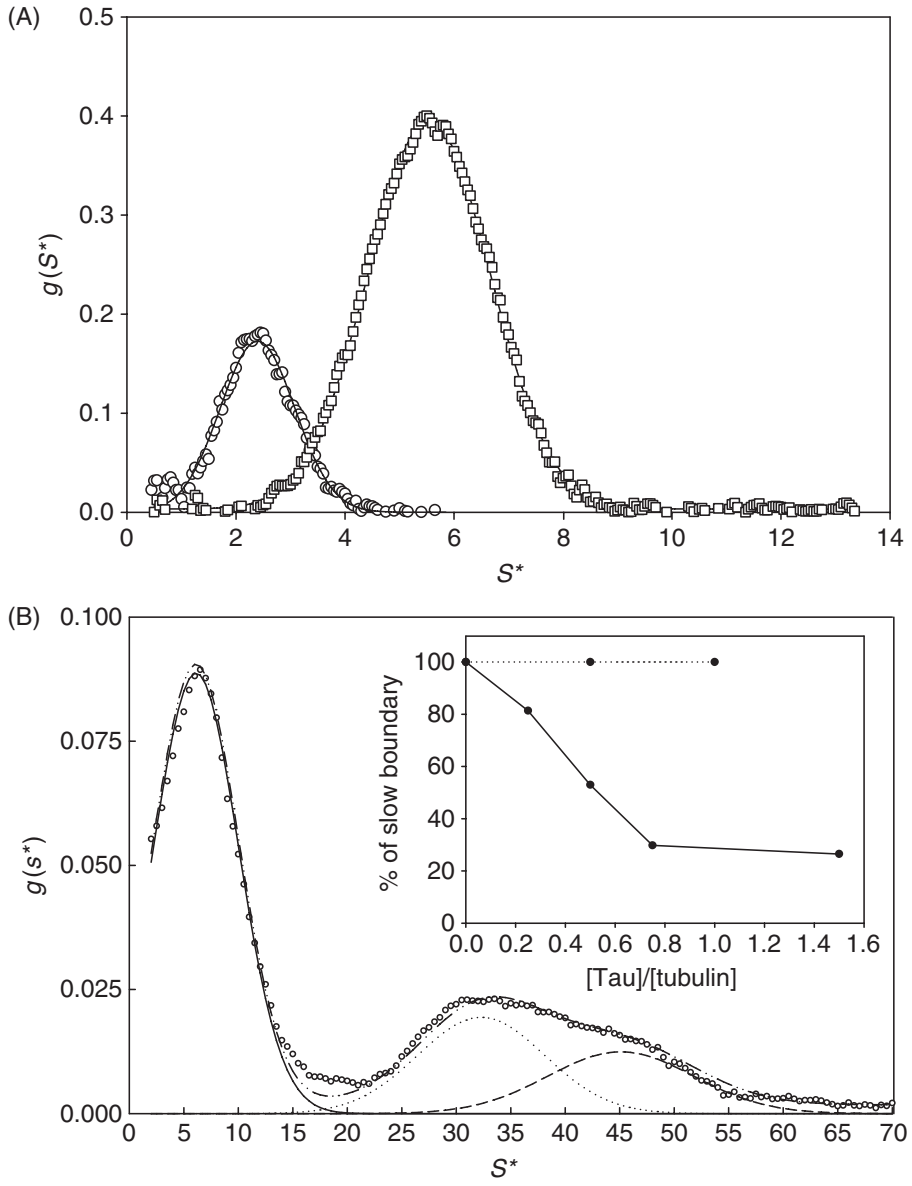

Fig. 2 Sedimentation velocity of tau tubulin interaction at 20°C. (A) Apparent sedimentation coefficient $g(s^*)$ distribution of tau protein (16 μM) alone (open circle) and tubulin dimers (15 μM) alone (open square) computed from the time derivative of the concentration profile by the method of Stafford (dark lines). (B) Apparent sedimentation coefficient $g(s^*)$ distribution of 15 μM tubulin mixed with 7.5 μM of tau. This distribution was analyzed by DCDT software, with three Gaussian curves representing three sedimentation boundaries respectively in the plane line, dotted line, and dashed line. Open circles represent experimental values. The long dashed dotted line represents the best fit curve. The inset shows the percentage of the slower boundaries (10 μM) tubulin in function of the tau/tubulin molar ratio for unphosphorylated (dark line); and phosphorylated tau (dotted line).

followed the effect of tau phosphorylation by the activated CDK2/cylcine A3 kinase complex (inset of Fig. 2B). In this condition, tau is phosphorylated on serine 202/threonine 205 and threonine 231/serine 235, which corresponds to the well-known Alzheimer epitopes AT8 and AT180, respectively. AUC clearly shows that within the same concentration range, phosphorylated tau is not able to form rings from tubulin dimers (dotted line).

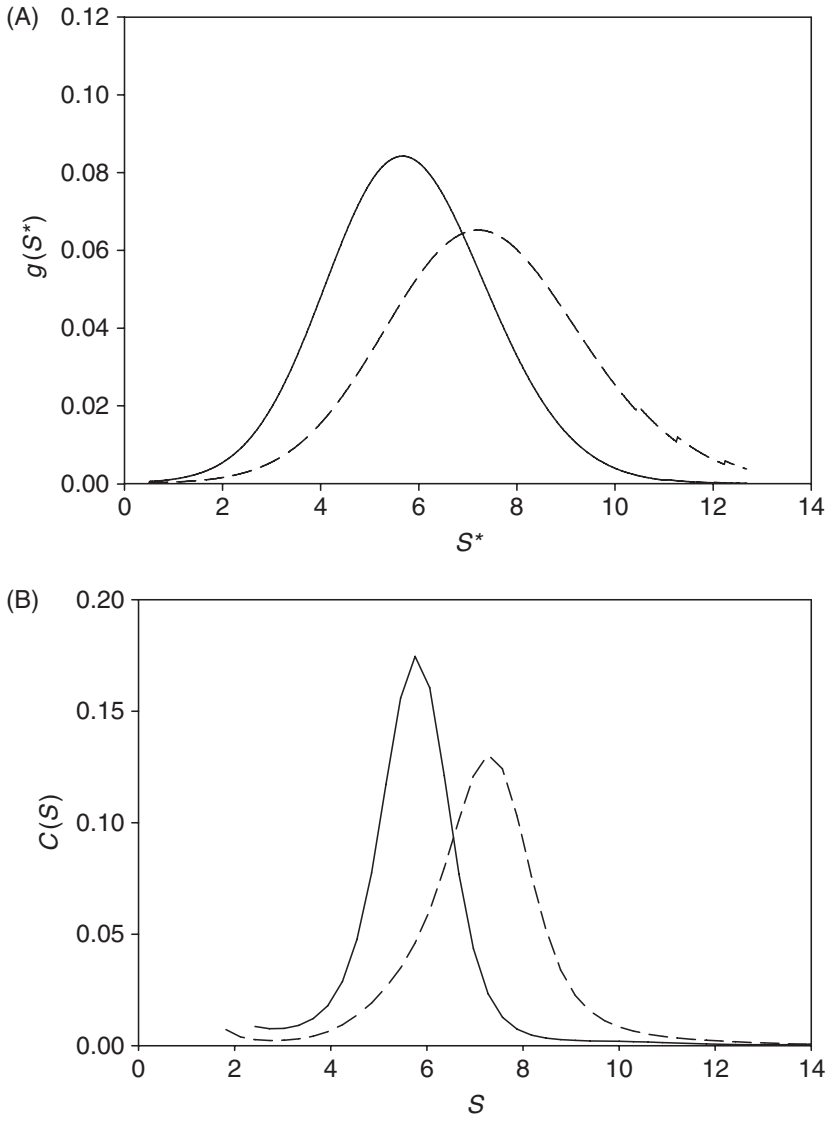

Fig. 3 Sedimentation velocity of tubulin alone (7 μM) (dark line) and with 4 μM of stathmin at 20°C analyzed by DCDT+ (A) or by Sedfit (B).

Another complex that can be easily analyzed by sedimentation velocity is the tubulin–stathmin complex (T2S). Tubulin sediments with an apparent sediment coefficient of 5.08 S whereas T2S, formed by two tubulin molecules linked by the helix of stathmin, sediments with a sediment coefficient of 7.7 S. Because stathmin has no aromatic residues, the absorbance measured in sedimentation run in the XLA was directly proportional to the tubulin concentration. As shown in Fig. 3, data analyzed by DCDT+ (A) or sedfit (B) gives similar results. In this case, AUC can be used to monitor the effect of other molecules like antimitotic drugs on the T2S formation. For example, we used it in complement with isothermal titration microcalorimetry, to monitor the oligomeric state of tubulin in presence of vinblastine, showing that stathmin induced the depolymerization of vinblastine oligomers to from T2S-like complexes. The thermodynamic parameters of this interaction were subsequently determined by ITC (Devred *et al.*, 2008).

B. Thermodynamic Parameters Determination of MAP–Tubulin Interaction

Having shown that stathmin bound to tubulin to form T2S complexes even in presence of vinblastine, we decided to study the thermodynamic parameters of its binding to tubulin as described previously (Honnappa *et al.*, 2003). If at a given temperature ΔH is too small to be measured, one needs to change the temperature to obtain a greater signal. This is the case for stathmin–tubulin interaction for which ΔH is close to null at 25°C. Having the choice of increasing the temperature or decreasing it, we chose to decrease it to 10°C, a temperature much more compatible with the long study of tubulin. Black curve in Fig. 4 shows the typical endothermic profile of a stathmin to tubulin binding at 10°C. On the upper panel each peak corresponds to the injection of 10 µl of stathmin at 76 µM into a tubulin dimer solution at 10 µM. The reaction heat measured for each injection, decreases as less and less tubulin is available for stathmin binding. After 15 injections, no further heat change is detected but the one due to stathmin dilution, which indicates that all stathmin is bound to tubulin. The lower panel shows the integrated heat peaks of reaction as a function of the stathmin/tubulin molar ratio. This representation of the abscissas enables us to

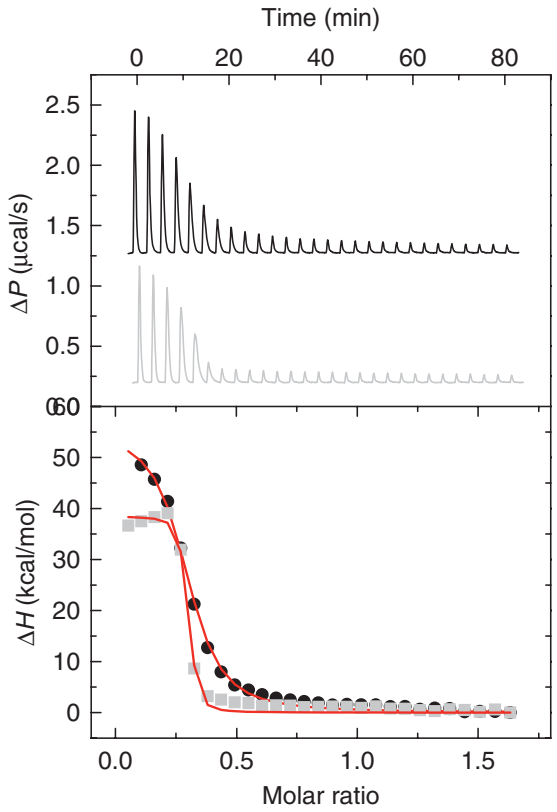

Fig. 4 Typical ITC curves of stathmin interaction with tubulin. Upper panel shows the raw data obtained for 25–30 injections, each of 10 µl, of stathmin (76 µM) into the sample cell containing tubulin (10 µM). The two titration curves were obtained during one set of experiments; the upper curve (black, which was translated upward for clarity purposes) corresponds to binding in absence of vinblastine, whereas the lower one (gray) corresponds to the binding in presence of vinblastine. Lower panel shows the integrated heats of reaction (symbols) in absence (black circles) and in presence of vinblastine (gray squares) with the best fit to the data (line). The measurements were carried out at 10°C in 20 mM NaPi, GTP 0.1 mM pH 6.5.

take into consideration the slight but not negligible change of tubulin concentration upon injection. Experiments carried out in phosphate buffer are minimally affected by a possible proton exchange and therefore the heat measured is solely due to the interaction. To analyze our stathmin–tubulin binding data we used the simplest model compatible with our raw data, based on previous studies reporting that stathmin binds two tubulin subunits with equal affinities under all conditions investigated by ITC (Honnappa *et al.*, 2003; Honnappa *et al.*, 2006). The analysis of the binding isotherm in their work and in ours is based on the model that assumes n independent and equal binding sites on stathmin for tubulin.

We then conducted the same experiment in presence of vinblastine, a drug known to trigger the formation of indefinite tubulin spiral polymers. Nevertheless, having shown that addition of stathmin leads to the same T2S-like complex and that no interfering signal from tubulin assembly or disassembly was observed, we analyzed our data with the same model. In our conditions, we could not take into account the linkage between drug binding and ligand-induced binding oligomer formation, nevertheless it enabled us to compare stathmin binding on free tubulin and on tubulin spiral oligomers.

In the presence of vinblastine, we encountered another issue when measuring stathmin binding to tubulin. Indeed, one of the limitations of ITC is the range of binding constants that can be determined directly. If C is the concentration of the macromolecule in the calorimeter cell and K_d is the dissociation constant measurable with accuracy, C should be in the range $K_d/100 \leq C \leq K_d \times 100$. Commonly used tubulin concentrations are between 20 μM and 1 μM for ITC which limits the range of measurable binding constants to $500\ M^{-1}$–$10^8\ M^{-1}$. When the association constant K_a exceeds $10^8\ M^{-1}$, the steepness of the isotherm does not allow accurate estimation of the binding constant. This is what happened in our study of stathmin binding to tubulin in the presence of vinblastine (see Fig. 4 bottom gray lines in the upper panel), which gives an underestimated binding constant that falls outside of the confidence interval of the apparatus. In that case, we used another thermodynamic path described in our study to calculate the more accurate binding constant (Devred *et al.*, 2008). But in some cases, when there is only one path possible, and the protein concentration in the cell cannot be lowered without loss of signal, we have to use another method to counter this problem. For example, competition or displacement titration calorimetry (Berland *et al.*, 1995; Sigurskjold, 2000) measures an apparent binding constant (K_{app}) corresponding to the displacement of a low-affinity ligand by a stronger one.

Such an approach was applied by our team to the measurement of coumarin binding to a bacterial protein DNA gyrase (Lafitte *et al.*, 2002), and could have been used in the case of stathmin–tubulin binding in presence of vinblastine if no other thermodynamical path was available. It would have implied the existence of another MAP or mutant of lower affinity for tubulin by site directed mutagenesis. Let us consider the use of a stathmin mutant (L_1) with a lower binding affinity for tubulin than stathmin (L_2) in presence of vinblastine. The fairly simple protocol is first to obtain the binding parameters of L_1 using the standard procedure as previously described. Then the tubulin–VLB would be saturated with the low-affinity ligand L_1 introduced into the calorimeter cell and then titrated with aliquots of high-affinity ligand L_2. The titration curve would be fitted to give an apparent binding constant, corresponding to the displacement of L_1 by L_2. Then, knowing the binding constant

K_1 of L_1, we could have estimated the value of the binding constant K_2 of normal stathmin for tubulin from the equation $K_2 = K_{app}(1 + K_1[L_1])$. This analysis derives from the rigorous analysis of Sigurskjold *et al.* which applied least-squares nonlinear regression method for the characterization of such displacement titration (Sigurskjold, 2000). Using this method binding constants up to 10^{13} M^{-1} have been measured.

As we mentioned earlier it is often useful to carry out the binding measurement at different temperature to obtain the change in heat capacity of the binding (ΔC_p). As we have already mentioned, heat capacity corresponds to the increase in energy with temperature: $C_p = dH/dT$, but it can also be defined as the temperature dependence of the entropy $C_p = T\, dS/dT$. Therefore, change in heat capacity upon binding (ΔC_p) is calculated using the following equations: $\Delta C_p = d\Delta H/dT$ or $\Delta C_p = T\, d\Delta S/dT$. This change in the heat capacity of binding (ΔC_p) is related to solvatation changes between two states of a system and can be determined by ITC measurements performed over a range of temperatures. This parameter is important for understanding how a protein adapts to the incorporation of the ligand. Upon binding, conformational changes can expose or hide apolar surfaces, resulting in a positive (exposure) or negative (hiding) contribution to ΔC_p (Jelesarov and Bosshard, 1999). In addition, the ligand binding decreases the protein surface accessibility to the solvent and hides apolar surfaces that are responsible for the major positive contribution to ΔC_p (Jelesarov and Bosshard, 1999).

ITC measurements have to be carried out at least at four temperatures on the wider temperature range possible (usually between 10 and 40°C) to avoid protein denaturation. It could be useful to perform a differential scanning calorimetry (DSC) run prior to a ΔC_p measurements to determine the starting temperature for protein unfolding. For tubulin, Diaz *et al.* (1993) performed DSC experiments in PEDTA buffer pH 6.7 in various conditions of magnesium and GTP/GDP concentrations. No denaturation was observed below 40°C. Therefore, it could be reasonable to choose 35°C as the highest temperature for performing the ITC measurements. The ΔH of binding is then plotted against temperature, and the data is fitted to a linear function to obtain the ΔC_p of binding. Interpretation of the biological significance of ΔC_p relies on physical but also empirical rules (Prabhu and Sharp, 2005). First, the sign of ΔC_p distinguishes apolar (+) from polar (–) solvation (Privalov and Gill, 1988), a positive ΔC_p, rather than negative ΔS, is now considered the signature of the hydrophobic effect. Second, solvation of polar groups found in proteins is characterized by both negative ΔC_p and ΔS at room temperature (Murphy *et al.*, 1990). Third, globular protein unfolding usually has a positive ΔC_p. This type of analysis has been applied to ligand binding to tubulin by Das *et al.* (2009) who have shown that that the enthalpy of association of indanocine with tubulin is negative and occurs with a negative heat capacity change ($\Delta C_p = -175.1$ cal mol^{-1} K^{-1}). It has also been applied to stathmin binding to tubulin to form a T2S complex (Honnappa *et al.*, 2003). The tubulin–stathmin binding reaction was monitored as a function of temperature. The reaction enthalpy was found to be endothermic at low temperatures and decreased linearly with temperature. Extrapolation to higher temperatures predicts $\Delta H = 0$ kcal/mol at 28°C and exothermic above this temperature. Hence, below 28°C the interaction between tubulin and stathmin is completely entropy driven, above this temperature both enthalpy and entropy contribute favorably to the binding reaction. The resulting molar heat capacity change of the

binding reaction is largely negative ($\Delta C_p = -860$ cal mol^{-1} K^{-1}), which is indicative of a hydrophobic reaction (removal of nonpolar surface from water) along with T2S complex formation.

In addition, in a recent paper we showed that the ΔC_p values of vinblastine binding in absence or presence of stathmin are also negative: -388 ± 32 cal mol^{-1} K^{-1} for vinblastine binding to tubulin and -1052 ± 56 cal mol^{-1} K^{-1} for VLB binding to T2S (Devred *et al.*, 2008). Since the VLB site on tubulin is the same in T2S as in VLB-induced oligomers (Gigant *et al.*, 2005), this difference in the ΔC_p observed in the two binding processes depends on the presence of stathmin, and can be explained by the positive contribution to ΔC_p from the burying of inter-tubulin interface hydrophobic surfaces during VLB-induced tubulin oligomerization (Makarov *et al.*, 2007). Moreover, these values of ΔC_p enabled us to calculate $\Delta H = 2$ kcal/mol for VLB binding to tubulin and $\Delta H = -20$ kcal/mol for VLB binding to T2S at 37°C. These results indicate that at the physiological temperature stathmin changes the thermodynamic mode of VLB binding to tubulin to an enthalpy-driven one, thus contributing to the observed increase in affinity of VLB to tubulin.

Since tau induces polymers even in "non-polymerization conditions" as demonstrated by AUC (Devred *et al.*, 2004), we performed co-sedimentation assay rather than ITC to characterize tau binding to tubulin. Using this approach with non-stabilized microtubules, we demonstrated that tau-induced tubulin assembly was following a ligand-induced mechanism rather than a ligand-stabilized mechanism. Then, in order to measure tau-binding parameters to tubulin, we used taxol-stablized MTs. In both cases we used the different sedimentation properties between free tau (a 45 kDa protein) and MTs-bound tau in a co-sedimentation assay. Preformed taxol-stabilized MTs were titrated with various tau concentrations at 20°C. By centrifuging samples through a glycerol cushion to eliminate unspecific binding, supernatants and pellet were separated and analyzed by SDS-PAGE to determine the fraction of bound and free tau. *B* (bound tau concentration divided by total tubulin concentration) was divided by free tau concentration *F* and plotted versus *B* in a Scatchard plot representation (Fig. 5). Data analysis by linear regression gives a slope corresponding to an association constant $K_a = 7.8 \pm 0.2 \times 10^5$ M^{-1} with 2.8 ± 0.3 identical binding sites. Fitting the same data plotted as a saturation curve (inset of Fig. 5)

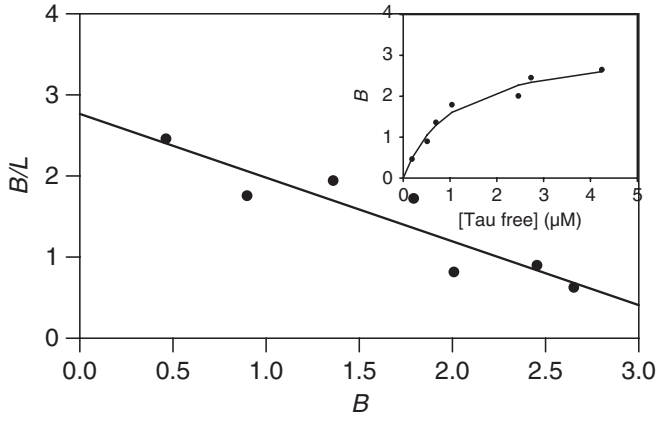

Fig. 5 Scatchard analysis of the co-sedimentation assay with 5 μM of MTs solution mixed with various tau concentrations. Inset: similar data analysed by saturation analysis.

leads to a dissociation constant of 1.1 ± 0.3 μM which corresponds to a similar value of association constant (9.4×10^5 M^{-1}).

This method is limited by the SDS-PAGE sensitivity, which is too low for tau concentration below 2 μM. In the range of concentration covered by SDS-PAGE, we cannot determine association constants greater than 10^7 M^{-1}. The stoichiometry close to three moles of tau for one mole of tubulin obtained by co-sedimentation suggests the presence of a tau accumulation on the MT wall. This accumulation could be suppressed when we performed co-sedimentation assays in the absence of DTT. Under these conditions, an intramolecular sulfide bridge is formed that blocks tau accumulation on MT because the stoichiometry decreases to one with a slight decrease of affinity constant (Sillen *et al.*, 2007). In order to measure the binding of the first tau to the microtubule wall, as opposed to the two subsequent events, we used FRET with tau cysteines labeled with acrylodan as previously described (Makrides *et al.*, 2004). We exploited the energy transfer between tryptophan/tyrosine residues of tubulin as donors and the fluorophore acrylodan on tau as acceptor. Since the tubulin–tau distance is comparable to the Förster distance, i.e., typically in the range of 20–60 Å, FRET provides a powerful and complementary tool to quantify the interaction between microtubule and tau. Titration of a fixed concentration of MTs (1 μM) with various concentration of acrylodan-labeled tau gave a values of $K_d = 20 \pm 4$ nM and a stoichiometry $n = 0.40 \pm 0.04$ of tau binding sites per tubulin dimer, in good agreement with literature (Makrides *et al.*, 2004). The discrepancy with the co-sedimentation results therefore suggests that FRET only accounts for the direct tau/MT interaction, whereas the co-sedimentation assay detects all bound tau protein, including the molecules that interact far away from tubulin aromatic residues, possibly via a tau–tau interaction (Sillen *et al.*, 2007). FRET is thus appropriate to study the effect of the most important posttranslational modification, the phosphorylation, on the direct tau–MT interaction. When tau is phosphorylated on the serine 214 by PKA *in vitro*, its binding is reduced 100-fold (Sillen *et al.*, 2007). By contrast, tau phosphorylation on Alzheimer epitope AT8 and AT180, does not modify its affinity (Amniai *et al.*, 2009). It is well known that tau binding on MTs is related to its induction and stabilization of MTs functions. Nevertheless, in recent studies (Amniai *et al.*, 2009), AUC and FRET enabled us to demonstrated that tau phosphorylated at epitope AT8 and AT180 lost its ability to induced MTs and ring formation even though its affinity for MTs remained unchanged. These results were confirmed by the use of tau mutants where only one epitope is maintain by replacement of the serine and threonine of the other epitope by alanines. We found that the presence of only one epitope (AT8 or AT180) is not sufficient to divert tau from its function.

C. Detailing the MAP–MT Interface: NMR

Whereas the above-mentioned methods can demonstrate the formation of a complex, determine its size, shape and stoechiometry, and can eventually yield numerical values for the thermodynamic parameters that characterize the complex, mechanistic details at the atomic level are general missing. The method of choice to provide such details is X-ray crystallography, as beautifully exemplified by the high-resolution structures of the RB3 SLD complexed to two tubulin dimers (Gigant *et al.*, 2000; Gigant *et al.*, 2005; Ravelli *et al.*, 2004). These structures allow the observation of

the RB3 helix with high resolution and detail all the intervening interactions (with a view on the individual hydrogen bonds, aromatic stacking interactions, etc.). Unfortunately, crystal structures of tau bound to the tubulin surface are currently lacking, despite intense efforts of several groups. Structures at the atomic level of tau in its complex with whatever form of tubulin are therefore still missing. As a consequence, we lack a deeper understanding on how tau stabilizes the microtubule, and how phosphorylation regulates this functional aspect. High-resolution metal-shadowing and cryo-electron microscopy showed that tau binds mainly to the outside of the microtubules (Santarella *et al.*, 2004), but did not give any detailed insight in the molecular interactions that underlie the association.

NMR of the MAPs and their complexes with microtubules has only very recently been reported. Despite some early work describing the observation of NMR signals from the flexible polyglutamate tails of tubulin (Reed *et al.*, 1992), MAPs such as tau were thought to be inaccessible for NMR studies due to their size and natively unfolded structure, rendering a sequence specific assignment impossible. We, however, realized that accepting this natively unfolded structure implied that at least the carbon chemical shifts were known. Tracing back the amide correlations from these carbon Cα and Cβ chemical shifts, we obtained first a partial assignment of full-length tau (Lippens *et al.*, 2004), that we then completed by a strategy dubbed "peptide mapping by NMR." In the latter approach, we superposed the $^{1}H,^{15}N$ spectra of small tau peptides recorded at natural abundance with the spectrum of full-length tau. Good overlap allowed us to complete the assignment, and equally provided a definition of the natively unfolded structure of tau (Smet *et al.*, 2004). Further improvements came by the use of higher field and lower temperature. As an example, we show the spectra of the same fragment of tau at 800 MHz and 4°C versus at 600 MHz and 20°C, where one can easily see the spectral improvement produced by increasing the field strength and lowering the temperature (Fig. 6).

Taking into account the experimental considerations mentioned above, in our studies of complexes between tau and taxol-stabilized microtubules, we measured a single ^{1}H, ^{15}N HSQC on a 5 μM ^{15}N-labeled tau sample in its complex with 20 μM tubulin assembled into taxol-stabilized MTs. From the disappearance of resonances in the overnight spectrum, we concluded that the region of direct physical interaction between tau and the MT surface spans the tau fragment from Ser214 to Thr377 (Sillen *et al.*, 2007). Although we did observe zones of intermediate intensity between the invisible interface and the flexible tails of tau, we could show that these intermediate regions were due to the anisotropic tumbling of the amino acids involved. This hypothesis was confirmed by the fact that over-expression of this fragment and affinity measurement through acrylodan labeling and FRET titration indeed showed that the fragment bound with the same affinity as full-length tau.

Will NMR be able to give detailed structural information on how tau binds to the MT surface? This would certainly be a first step toward understanding how it favors the assembly of tubulin into microtubules, and also how phosphorylation regulates this process. Working with microtubules will remain challenging, because even with full deuteration of tau, the bound part on such large systems broadens beyond detection. We show this in Fig. 7 with a TauF1 fragment spanning residues 169–441. Only those parts that project from the surface maintain detectable intensity. Recently, solid state NMR has given some further insight into the Cap-Gly protein and its interaction with microtubules (Sun *et al.*, 2009), and might in the future

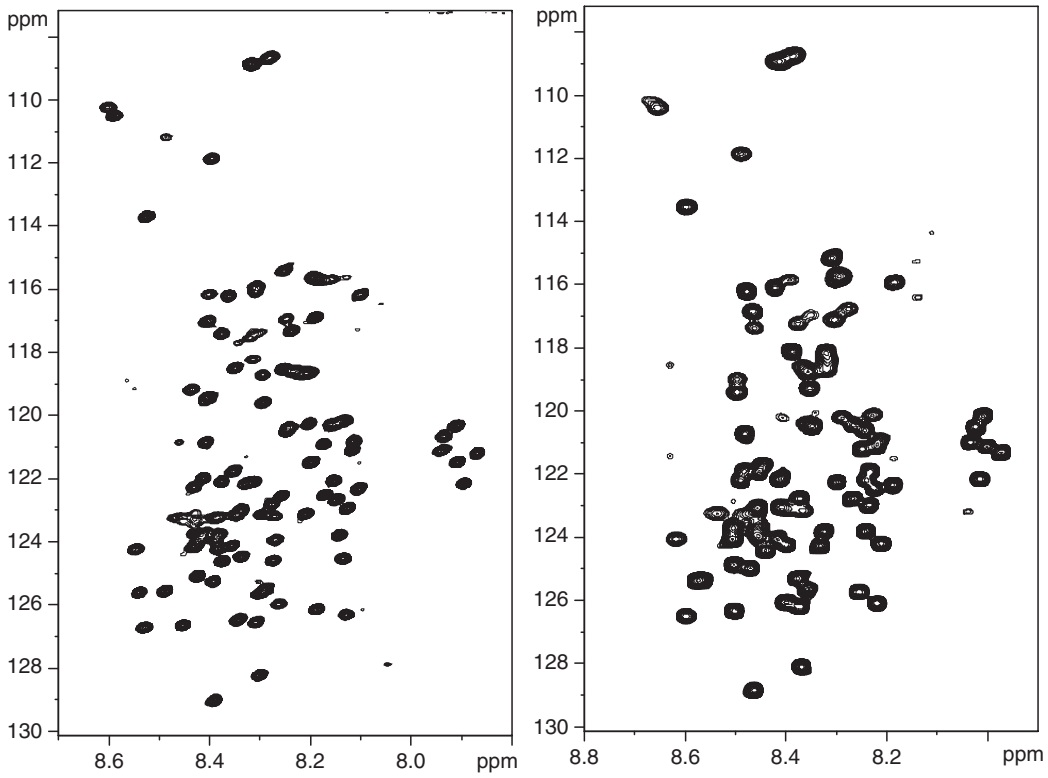

Fig. 6 HSQC spectra of a tau fragment [208–324] at 4°C and 800 MHz (left) or 20°C and 600 MHz (right), illustrating the gain in resolution of both a lower temperature and higher field.

evolve toward a technique that can handle samples of this size. However, current believe is that working with well-defined rings or other systems in which the sample heterogeneity due to polymerization is less problematic will be the more promising route to answer these challenging questions.

V. Concluding Remarks

Characterizing the molecular mechanisms of MT–MAP interaction is highly relevant both to understanding their biological functions and their deregulation leading to severe pathologies such as cancer or neurodegenerative diseases. The microtubule cytoskeleton is a network for which specific care must be taken because of the peculiar physicochemical properties of its main constituents. Tubulin, in addition to its natural fragility, needs to be handled with care because of its capability to self-assemble into a wide variety of polymers; tau and stathmin cannot be traced easily because of their lack of aromatic residues; tau is natively unstructured. All these apparent sources of concern in a protein–protein interaction study actually became advantages to characterize the thermodynamics of MAPs–tubulin complex formation. We used the peculiar properties of the three proteins studied (tau, stathmin, and tubulin) to detail the most appropriate combination of methods (AUC, ITC, FRET and NMR, as well as co-sedimentation) to characterize the complexes formed, to determine the thermodynamic parameters of these interactions and to detail the MAP/MT interface. This biophysical approach has allowed us to give new insight into the molecular mechanisms that govern MAPs

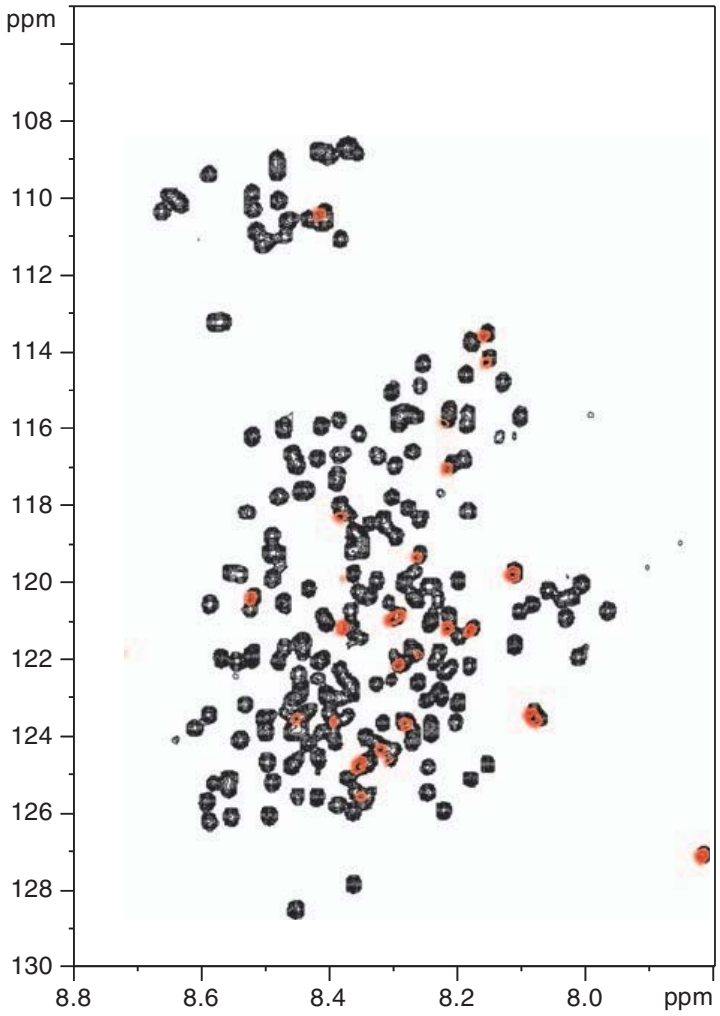

Fig. 7 HSQC spectra of a tau fragment [169–441] (TauF1) uniformly labelled with ^{15}N and ^{2}D, free in solution (black) or in its complex with paclitaxel-stabilized microtubules (red). For the latter spectra, 10 μM TauF1 was added to 40 μM polymerized tubulin. Only the extreme C-terminal of the tau fragment maintains mobility in this complex. (See Plate no. 30 in the Color Plate Section.)

action on MT network. This will not only shed new light on the role of this crucial family of proteins in the biology of the cell, but will also hopefully open new paths to enhance the therapeutic efficiency of microtubule-targeting drugs in cancers therapies and neurodegenerative diseases prevention.

Acknowledgments

We thank Diane Allegro, Robert Michel, and Soazig Douillard for technical assistance. This work was supported by grants from Association pour la Recherche contre le Cancer (n° 1035), from the CNRS (PICS n° 3841), and by an ANR-05-blanc-6320-01 grant.

References

Alday, P. H., and Correia, J. J. (2009). Macromolecular interaction of halichondrin B analogues eribulin (E7389) and ER-076349 with tubulin by analytical ultracentrifugation. *Biochemistry* **48**, 7927–7938.

Alli, E., Bash-Babula, J., Yang, J. M., and Hait, W. N. (2002). Effect of stathmin on the sensitivity to antimicrotubule drugs in human breast cancer. *Cancer Res.* **62**, 6864–6869.

Alli, E., Yang, J. M., Ford, J. M., and Hait, W. N. (2007a). Reversal of stathmin-mediated resistance to paclitaxel and vinblastine in human breast carcinoma cells. *Mol. Pharmacol.* **71**, 1233–1240.

Alli, E., Yang, J. M., and Hait, W. N. (2007b). Silencing of stathmin induces tumor-suppressor function in breast cancer cell lines harboring mutant p53. *Oncogene* **26**, 1003–1012.

Amniai, L., Barbier, P., Sillen, A., Wieruszeski, J. M., Peyrot, V., Lippens, G., and Landrieu, I. (2009). Alzheimer disease specific phosphoepitopes of Tau interfere with assembly of tubulin but not binding to microtubules. *FASEB J.* **23**, 1146–1152.

Andreu, J. M. (2007). Large scale purification of brain tubulin with the modified Weisenberg procedure. *Methods Mol. Med.* **137**, 17–28.

Barbier, P., Gregoire, C., Devred, F., Sarrazin, M., and Peyrot, V. (2001). *In vitro* effect of cryptophycin 52 on microtubule assembly and tubulin: Molecular modeling of the mechanism of action of a new antimitotic drug. *Biochemistry* **40**, 13510–13519.

Barbier, P., Peyrot, V., Dumortier, C., D'Hoore, A., Rener, G. A., and Engelborghs, Y. (1996). Kinetics of association and dissociation of two enantiomers, NSC 613863 (R)-(+) and NSC 613862 (S)-(-) (CI 980), to tubulin. *Biochemistry* **35**, 2008–2015.

Barbier, P., Peyrot, V., Leynadier, D., and Andreu, J. M. (1998). The active GTP- and ground GDP-liganded states of tubulin are distinguished by the binding of chiral isomers of ethyl 5-amino-2-methyl-1,2-dihydro-3-phenylpyrido[3,4-b]pyrazin-7-yl carbamate. *Biochemistry* **37**, 758–768.

Barbier, P., Peyrot, V., Sarrazin, M., Rener, G. A., and Briand, C. (1995). Differential effects of ethyl 5-amino-2-methyl-1,2-dihydro-3-phenylpyrido[3,4-b]pyrazin-7-yl carbamate analogs modified at position C2 on tubulin polymerization, binding, and conformational changes. *Biochemistry* **34**, 16821–16829.

Berland, C. R., Sigurskjold, B. W., Stoffer, B., Frandsen, T. P., and Svensson, B. (1995). Thermodynamics of inhibitor binding to mutant forms of glucoamylase from Aspergillus niger determined by isothermal titration calorimetry. *Biochemistry* **34**, 10153–10161.

Bhattacharya, A., Bhattacharyya, B., and Roy, S. (1994). Magnesium-induced structural changes in tubulin. *J. Biol. Chem.* **269**, 28655–28661.

Bhattacharya, A., Bhattacharyya, B., and Roy, S. (1996). Fluorescence energy transfer measurement of distances between ligand binding sites of tubulin and its implication for protein–protein interaction. *Protein Sci.* **5**, 2029–2036.

Bhattacharyya, A., Bhattacharyya, B., and Roy, S. (1993). A study of colchicine tubulin complex by donor quenching of fluorescence energy transfer. *Eur. J. Biochem.* **216**, 757–761.

Biernat, J., Mandelkow, E. M., Schroter, C., Lichtenberg-Kraag, B., Steiner, B., Berling, B., Meyer, H., Mercken, M., Vandermeeren, A., Goedert, M., et al. (1992). The switch of tau protein to an Alzheimer-like state includes the phosphorylation of two serine-proline motifs upstream of the microtubule binding region. *EMBO J.* **11**, 1593–1597.

Bonne, D., Heusele, C., Simon, C., and Pantaloni, D. (1985). 4′,6-Diamidino-2-phenylindole, a fluorescent probe for tubulin and microtubules. *J. Biol. Chem.* **260**, 2819–2825.

Borisy, G. G., Olmsted, J. B., and Klugman, R. A. (1972). *In vitro* aggregation of cytoplasmic microtubule subunits. *Proc. Natl. Acad. Sci. U. S.A.* **69**, 2890–2894.

Briand, C., Sarrazin, M., Peyrot, V., Gilli, R., Bourdeaux, M., and Sari, J. C. (1982). Study of the interaction between human serum albumin and some cephalosporins. *Mol. Pharmacol.* **21**, 92–99.

Buey, R. M., Diaz, J. F., Andreu, J. M., O'Brate, A., Giannakakou, P., Nicolaou, K. C., Sasmal, P. K., Ritzen, A., and Namoto, K. (2004). Interaction of epothilone analogs with the paclitaxel binding site: Relationship between binding affinity, microtubule stabilization, and cytotoxicity. *Chem. Biol.* **11**, 225–236.

Bujalowski, W., and Lohman, T. M. (1987). A general method of analysis of ligand–macromolecule equilibria using a spectroscopic signal from the ligand to monitor binding. Application to *Escherichia coli* single-strand binding protein–nucleic acid interactions. *Biochemistry* **26**, 3099–3106.

Charbaut, E., Curmi, P. A., Ozon, S., Lachkar, S., Redeker, V., and Sobel, A. (2001). Stathmin family proteins display specific molecular and tubulin binding properties. *J. Biol. Chem.* **276**, 16146–16154.

Chatterjee, S. K., Barron, D. M., Vos, S., and Bane, S. (2001). Baccatin III induces assembly of purified tubulin into long microtubules. *Biochemistry* **40**, 6964–6970.

Christensen, J. J., Izatt, R. M., Hansen, L. D., and Partridge, J. M. (1966). Entropy titration. A calorimetric method for the determination of DG, DH and DS from a single thermodynamic tritration. *J. Phys. Chem.* **70**, 8.

Cleveland, D. W., Hwo, S. Y., and Kirschner, M. W. (1977). Purification of tau, a microtubule-associated protein that induces assembly of microtubules from purified tubulin. *J. Mol. Biol.* **116**, 207–225.

Curmi, P. A., Nogues, C., Lachkar, S., Carelle, N., Gonthier, M. P., Sobel, A., Lidereau, R., and Bieche, I. (2000). Overexpression of stathmin in breast carcinomas points out to highly proliferative tumours. *Br. J. Cancer* **82**, 142–150.

Das, L., Gupta, S., Dasgupta, D., Poddar, A., Janik, M. E., and Bhattacharyya, B. (2009). Binding of indanocine to the colchicine site on tubulin promotes fluorescence, and its binding parameters resemble those of the colchicine analogue AC. *Biochemistry* **48**, 1628–1635.

Devred, F., Barbier, P., Douillard, S., Monasterio, O., Andreu, J. M., and Peyrot, V. (2004). Tau induces ring and microtubule formation from alphabeta-tubulin dimers under nonassembly conditions. *Biochemistry* **43**, 10520–10531.

Devred, F., Tsvetkov, P. O., Barbier, P., Allegro, D., Horwitz, S. B., Makarov, A. A., and Peyrot, V. (2008). Stathmin/Op18 is a novel mediator of vinblastine activity. *FEBS Lett.* **582**, 2484–2488.

Diaz, J. F., Menendez, M., and Andreu, J. M. (1993). Thermodynamics of ligand-induced assembly of tubulin. *Biochemistry* **32**, 10067–10077.

Förster, T. (1948). Intermolecular energy migration and fluorescence. *Annalen der Physik.* **2**, 55–75 (translated by Knox R. S.).

Freire, E., van Osdol, W. W., Mayorga, O. L., and Sanchez-Ruiz, J. M. (1990). Calorimetrically determined dynamics of complex unfolding transitions in proteins. *Annu. Rev. Biophys. Biophys. Chem.* **19**, 159–188.

Freyer, M. W., and Lewis, E. A. (2008). Isothermal titration calorimetry: Experimental design, data analysis, and probing macromolecule/ligand binding and kinetic interactions. *Methods Cell Biol.* **84**, 79–113.

Friedrich, B., Gronberg, H., Landstrom, M., Gullberg, M., and Bergh, A. (1995). Differentiation-stage specific expression of oncoprotein 18 in human and rat prostatic adenocarcinoma. *Prostate* **27**, 102–109.

Frigon, R. P., and Timasheff, S. N. (1975a). Magnesium-induced self-association of calf brain tubulin. I. Stoichiometry. *Biochemistry* **14**, 4559–4566.

Frigon, R. P., and Timasheff, S. N. (1975b). Magnesium-induced self-association of calf brain tubulin. II. Thermodynamics. *Biochemistry* **14**, 4567–4573.

Frigon, R. P., Valenzuela, M. S., and Timasheff, S. N. (1974). Structure of a magnesium-induced polymer of calf brain microtubule protein. *Arch. Biochem. Biophys.* **165**, 442–443.

Garnier, C., Barbier, P., Devred, F., Rivas, G., and Peyrot, V. (2002). Hydrodynamic properties and quaternary structure of the 90 kDa heat-shock protein: Effects of divalent cations. *Biochemistry* **41**, 11770–11778.

Garnier, C., Barbier, P., Gilli, R., Lopez, C., Peyrot, V., and Briand, C. (1998). Heat-shock protein 90 (hsp90) binds *in vitro* to tubulin dimer and inhibits microtubule formation. *Biochem. Biophys. Res. Commun.* **250**, 414–419.

Ghosh, R., Gu, G., Tillman, E., Yuan, J., Wang, Y., Fazli, L., Rennie, P. S., and Kasper, S. (2007). Increased expression and differential phosphorylation of stathmin may promote prostate cancer progression. *Prostate* **67**, 1038–1052.

Gigant, B., Curmi, P. A., Martin-Barbey, C., Charbaut, E., Lachkar, S., Lebeau, L., Siavoshian, S., Sobel, A., and Knossow, M. (2000). The 4 A X-ray structure of a tubulin:stathmin-like domain complex. *Cell* **102**, 809–816.

Gigant, B., Wang, C., Ravelli, R. B., Roussi, F., Steinmetz, M. O., Curmi, P. A., Sobel, A., and Knossow, M. (2005). Structural basis for the regulation of tubulin by vinblastine. *Nature* **435**, 519–522.

Gilli, R., Lafitte, D., Lopez, C., Kilhoffer, M., Makarov, A., Briand, C., and Haiech, J. (1998). Thermodynamic analysis of calcium and magnesium binding to calmodulin. *Biochemistry* **37**, 5450–5456.

Gilli, R. M., Sari, J. C., Lopez, C. L., Rimet, O. S., and Briand, C. M. (1990). Comparative thermodynamic study of the interaction of some antifolates with dihydrofolate reductase. *Biochim. Biophys. Acta* **1040**, 245–250.

Gilli, R. M., Sari, J. C., Sica, L. M., and Briand, C. M. (1988). Thermodynamic study of the influence of NADPH on the binding of methotrexate and its metabolites to a mammalian dihydrofolate reductase. *Biochim. Biophys. Acta* **964**, 53–60.

Goedert, M., Jakes, R., Crowther, R. A., Cohen, P., Vanmechelen, E., Vandermeeren, M., and Cras, P. (1994). Epitope mapping of monoclonal antibodies to the paired helical filaments of Alzheimer's disease: Identification of phosphorylation sites in tau protein. *Biochem. J.* **301**(Pt 3), 871–877.

Goedert, M., Jakes, R., Qi, Z., Wang, J. H., and Cohen, P. (1995). Protein phosphatase 2A is the major enzyme in brain that dephosphorylates tau protein phosphorylated by proline-directed protein kinases or cyclic AMP-dependent protein kinase. *J. Neurochem.* **65**, 2804–2807.

Han, Y., Malak, H., Chaudhary, A. G., Chordia, M. D., Kingston, D. G., and Bane, S. (1998). Distances between the paclitaxel, colchicine, and exchangeable GTP binding sites on tubulin. *Biochemistry* **37**, 6636–6644.

Hasegawa, M., Morishima-Kawashima, M., Takio, K., Suzuki, M., Titani, K., and Ihara, Y. (1992). Protein sequence and mass spectrometric analyses of tau in the Alzheimer's disease brain. *J. Biol. Chem.* **267**, 17047–17054.

Hitt, A. L., Cross, A. R., and Williams, R. C., Jr. (1990). Microtubule solutions display nematic liquid crystalline structure. *J. Biol. Chem.* **265**, 1639–1647.

Hoffmann, R., Dawson, N. F., Wade, J. D., and Otvos, L., Jr. (1997). Oxidized and phosphorylated synthetic peptides corresponding to the second and third tubulin-binding repeats of the tau protein reveal structural features of paired helical filament assembly. *J. Pept. Res.* **50**, 132–142.

Honnappa, S., Cutting, B., Jahnke, W., Seelig, J., and Steinmetz, M. O. (2003). Thermodynamics of the Op18/stathmin-tubulin interaction. *J. Biol. Chem.* **278**, 38926–38934.

Honnappa, S., Jahnke, W., Seelig, J., and Steinmetz, M. O. (2006). Control of intrinsically disordered stathmin by multisite phosphorylation. *J. Biol. Chem.* **281**, 16078–16083.

Howard, W. D., and Timasheff, S. N. (1986). GDP state of tubulin: Stabilization of double rings. *Biochemistry* **25**, 8292–8300.

Iancu, C., Mistry, S. J., Arkin, S., and Atweh, G. F. (2000). Taxol and anti-stathmin therapy: A synergistic combination that targets the mitotic spindle. *Cancer Res.* **60**, 3537–3541.

Jelesarov, I., and Bosshard, H. R. (1999). Isothermal titration calorimetry and differential scanning calorimetry as complementary tools to investigate the energetics of biomolecular recognition. *J. Mol. Recognit.* **12**, 3–18.

Kung, C. E., and Reed, J. K. (1989). Fluorescent molecular rotors: A new class of probes for tubulin structure and assembly. *Biochemistry* **28**, 6678–6686.

Lafitte, D., Lamour, V., Tsvetkov, P. O., Makarov, A. A., Klich, M., Deprez, P., Moras, D., Briand, C., and Gilli, R. (2002). DNA gyrase interaction with coumarin-based inhibitors: The role of the hydroxybenzoate isopentenyl moiety and the 5′-methyl group of the noviose. *Biochemistry* **41**, 7217–7223.

Landrieu, I., Lacosse, L., Leroy, A., Wieruszeski, J. M., Trivelli, X., Sillen, A., Sibille, N., Schwalbe, H., Saxena, K., Langer, T., and Lippens, G. (2006). NMR analysis of a Tau phosphorylation pattern. *J. Am. Chem. Soc.* **128**, 3575–3583.

Laue, T. M., Shah, B. D., Ridgeway, T. M., and Pelletier, S. L. (1992). "Computer-Aided Interpretation of Analytical Sedimentation Data for Proteins in Analytical Ultracentrifugation." Royal Society of Chemistry, Cambridge, UK.

Lee, J. C., and Rajendran, S. (1994). "Studies of Macromolecular Interaction by Sedimentation Velocity." Birkhauser, Boston.

Lee, J. C., and Timasheff, S. N. (1974). Partial specific volumes and interactions with solvent components of proteins in guanidine hydrochloride. *Biochemistry* **13**, 257–265.

Leynadier, D., Peyrot, V., Sarrazin, M., Briand, C., Andreu, J. M., Rener, G. A., and Temple, C., Jr. (1993). Tubulin binding of two 1-deaza-7,8-dihydropteridines with different biological properties: Enantiomers NSC 613862 (S)-(-) and NSC 613863 (R)-(+). *Biochemistry* **32**, 10675–10682.

Lippens, G., Wieruszeski, J. M., Leroy, A., Smet, C., Sillen, A., Buee, L., and Landrieu, I. (2004). Proline-directed random-coil chemical shift values as a tool for the NMR assignment of the tau phosphorylation sites. *Chembiochem* **5**, 73–78.

Lobert, S., and Correia, J. J. (2007). Methods for studying vinca alkaloid interactions with tubulin. *Methods Mol. Med.* **137**, 261–280.

Lobert, S., Ingram, J. W., Hill, B. T., and Correia, J. J. (1998). A comparison of thermodynamic parameters for vinorelbine- and vinflunine-induced tubulin self-association by sedimentation velocity. *Mol. Pharmacol.* **53**, 908–915.

Makarov, A. A., Tsvetkov, P. O., Villard, C., Esquieu, D., Pourroy, B., Fahy, J., Braguer, D., Peyrot, V., and Lafitte, D. (2007). Vinflunine, a novel microtubule inhibitor, suppresses calmodulin interaction with the microtubule-associated protein STOP. *Biochemistry* **46**, 14899–14906.

Makrides, V., Massie, M. R., Feinstein, S. C., and Lew, J. (2004). Evidence for two distinct binding sites for tau on microtubules. *Proc. Natl. Acad. Sci. U.S.A.* **101**, 6746–6751.

Marcum, J. M., and Borisy, G. G. (1978). Characterization of microtubule protein oligomers by analytical ultracentrifugation. *J. Biol. Chem.* **253**, 2825–2833.

Martello, L. A., Verdier-Pinard, P., Shen, H. J., He, L., Torres, K., Orr, G. A., and Horwitz, S. B. (2003). Elevated levels of microtubule destabilizing factors in a Taxol-resistant/dependent A549 cell line with an alpha-tubulin mutation. *Cancer Res.* **63**, 1207–1213.

Mercken, M., Vandermeeren, M., Lubke, U., Six, J., Boons, J., Van de Voorde, A., Martin, J. J., and Gheuens, J. (1992). Monoclonal antibodies with selective specificity for Alzheimer Tau are directed against phosphatase-sensitive epitopes. *Acta Neuropathol.* **84**, 265–272.

Mistry, S. J., Bank, A., and Atweh, G. F. (2007). Synergistic antiangiogenic effects of stathmin inhibition and taxol exposure. *Mol. Cancer Res.* **5**, 773–782.

Mukrasch, M. D., Bibow, S., Korukottu, J., Jeganathan, S., Biernat, J., Griesinger, C., Mandelkow, E., and Zweckstetter, M. (2009). Structural polymorphism of 441-residue tau at single residue resolution. *PLoS Biol.* **7**, e34.

Murphy, K. P., Privalov, P. L., and Gill, S. J. (1990). Common features of protein unfolding and dissolution of hydrophobic compounds. *Science* **247**, 559–561.

Na, G. C., and Timasheff, S. N. (1980a). Stoichiometry of the vinblastine-induced self-association of calf brain tubulin. *Biochemistry* **19**, 1347–1354.

Na, G. C., and Timasheff, S. N. (1980b). Thermodynamic linkage between tubulin self-association and the binding of vinblastine. *Biochemistry* **19**, 1355–1365.

Na, G. C., and Timasheff, S. N. (1986a). Interaction of vinblastine with calf brain tubulin: Effects of magnesium ions. *Biochemistry* **25**, 6222–6228.

Na, G. C., and Timasheff, S. N. (1986b). Interaction of vinblastine with calf brain tubulin: Multiple equilibria. *Biochemistry* **25**, 6214–6222.

Pervushin, K., Riek, R., Wider, G., and Wuthrich, K. (1997). Attenuated T2 relaxation by mutual cancellation of dipole–dipole coupling and chemical shift anisotropy indicates an avenue to NMR structures of very large biological macromolecules in solution. *Proc. Natl. Acad. Sci. U.S.A.* **94**, 12366–12371.

Peyrot, V., Briand, C., and Andreu, J. M. (1990). C-terminal cleavage of tubulin by subtilisin enhances ring formation. *Arch. Biochem. Biophys.* **279**, 328–337.

Peyrot, V., Briand, C., and Andreu, J. M. (1991). Limited proteolysis of tubulin by subtilisin induces ring formation. In "The Living cell in four dimensions." (G. Paillotin, ed.), Vol. 1, pp. 181–186. American Institute of Physics, Gif sur Yvette, France.

Peyrot, V., Leynadier, D., Sarrazin, M., Briand, C., Menendez, M., Laynez, J., and Andreu, J. M. (1992). Mechanism of binding of the new antimitotic drug MDL 27048 to the colchicine site of tubulin: Equilibrium studies. *Biochemistry* **31**, 11125–11132.

Philo, J. S. (2000). A method for directly fitting the time derivative of sedimentation velocity data and an alternative algorithm for calculating sedimentation coefficient distribution functions. *Anal. Biochem.* **279**, 151–163.

Pieulle, L., Morelli, X., Gallice, P., Lojou, E., Barbier, P., Czjzek, M., Bianco, P., Guerlesquin, F., and Hatchikian, E. C. (2005). The type I/type II cytochrome c3 complex: An electron transfer link in the hydrogen-sulfate reduction pathway. *J. Mol. Biol.* **354**, 73–90.

Prabhu, N. V., and Sharp, K. A. (2005). Heat capacity in proteins. *Annu. Rev. Phys. Chem.* **56**, 521–548.

Prasad, A. R., Luduena, R. F., and Horowitz, P. M. (1986). Detection of energy transfer between tryptophan residues in the tubulin molecule and bound bis(8-anilinonaphthalene-1-sulfonate), an inhibitor of microtubule assembly, that binds to a flexible region on tubulin. *Biochemistry* **25**, 3536–3540.

Price, D. K., Ball, J. R., Bahrani-Mostafavi, Z., Vachris, J. C., Kaufman, J. S., Naumann, R. W., Higgins, R. V., and Hall, J. B. (2000). The phosphoprotein Op18/stathmin is differentially expressed in ovarian cancer. *Cancer Invest.* **18**, 722–730.

Privalov, P. L., and Gill, S. J. (1988). Stability of protein structure and hydrophobic interaction. *Adv. Protein Chem.* **39**, 191–234.

Rappl, C., Barbier, P., Bourgarel-Rey, V., Gregoire, C., Gilli, R., Carre, M., Combes, S., Finet, J. P., and Peyrot, V. (2006). Interaction of 4-arylcoumarin analogues of combretastatins with microtubule network of HBL100 cells and binding to tubulin. *Biochemistry* **45**, 9210–9218.

Ravelli, R. B., Gigant, B., Curmi, P. A., Jourdain, I., Lachkar, S., Sobel, A., and Knossow, M. (2004). Insight into tubulin regulation from a complex with colchicine and a stathmin-like domain. *Nature* **428**, 198–202.

Reed, J., Hull, W. E., Ponstingl, H., and Himes, R. H. (1992). Conformational properties of the beta (400–436) and beta(400–445) C-terminal peptides of porcine brain tubulin. *Biochemistry* **31**, 11888–11895.

Santarella, R. A., Skiniotis, G., Goldie, K. N., Tittmann, P., Gross, H., Mandelkow, E. M., Mandelkow, E., and Hoenger, A. (2004). Surface-decoration of microtubules by human tau. *J. Mol. Biol.* **339**, 539–553.

Scheele, R. B., and Borisy, G. G. (1978). Electron microscopy of metal-shadowed and negatively stained microtubule protein. Structure of the 30 S oligomer. *J. Biol. Chem.* **253**, 2846–2851.

Scott, D. J., and Schuck, P. (2005). "A Brief Introduction to the Analytical Ultracentrifugation of Protein for Beginners." Royal Society of Chemistry, Cambridge, UK.

Sibille, N., Sillen, A., Leroy, A., Wieruszeski, J. M., Mulloy, B., Landrieu, I., and Lippens, G. (2006). Structural impact of heparin binding to full-length Tau as studied by NMR spectroscopy. *Biochemistry* **45**, 12560–12572.

Sigurskjold, B. W. (2000). Exact analysis of competition ligand binding by displacement isothermal titration calorimetry. *Anal. Biochem.* **277**, 260–266.

Sillen, A., Barbier, P., Landrieu, I., Lefebvre, S., Wieruszeski, J. M., Leroy, A., Peyrot, V., and Lippens, G. (2007). NMR investigation of the interaction between the neuronal protein tau and the microtubules. *Biochemistry* **46**, 3055–3064.

Smet, C., Leroy, A., Sillen, A., Wieruszeski, J. M., Landrieu, I., and Lippens, G. (2004). Accepting its random coil nature allows a partial NMR assignment of the neuronal Tau protein. *Chembiochem*. **5**(**12**), 1639–1646.

Soto, C., Rodriguez, P. H., and Monasterio, O. (1996). Calcium and gadolinium ions stimulate the GTPase activity of purified chicken brain tubulin through a conformational change. *Biochemistry* **35**, 6337–6344.

Stafford, W. F., 3rd (1992). Boundary analysis in sedimentation transport experiments: A procedure for obtaining sedimentation coefficient distributions using the time derivative of the concentration profile. *Anal. Biochem.* **203**, 295–301.

Sun, S., Siglin, A., Williams, J. C., and Polenova, T. (2009). Solid-state and solution NMR studies of the CAP-Gly domain of mammalian dynactin and its interaction with microtubules. *J Am Chem Soc.* **131**(**29**), 10113–10126.

Trojanowski, J. Q., and Lee, V. M. (2002). The role of tau in Alzheimer's disease. *Med. Clin. North Am.* **86**, 615–627.

Vallee, R. B., and Borisy, G. G. (1978). The non-tubulin component of microtubule protein oligomers. Effect on self-association and hydrodynamic properties. *J. Biol. Chem.* **253**, 2834–2845.

Ward, L. D., Seckler, R., and Timasheff, S. N. (1994). Energy transfer studies of the distances between the colchicine, ruthenium red, and bisANS binding sites on calf brain tubulin. *Biochemistry* **33**, 11900–11908.

Ward, L. D., and Timasheff, S. N. (1988). Energy-transfer studies of the distance between the high-affinity metal binding site and the colchicine and 8-anilino-1-naphthalenesulfonic acid binding sites on calf brain tubulin. *Biochemistry* **27**, 1508–1514.

Xi, W., Rui, W., Fang, L., Ke, D., Ping, G., and Hui-Zhong, Z. (2009). Expression of stathmin/op18 as a significant prognostic factor for cervical carcinoma patients. *J. Cancer Res. Clin. Oncol.* **135**, 837–846.

Zheng-Fischhofer, Q., Biernat, J., Mandelkow, E. M., Illenberger, S., Godemann, R., and Mandelkow, E. (1998). Sequential phosphorylation of Tau by glycogen synthase kinase-3beta and protein kinase A at Thr212 and Ser214 generates the Alzheimer-specific epitope of antibody AT100 and requires a paired-helical-filament-like conformation. *Eur. J. Biochem.* **252**, 542–552.